Acoustic streaming in pulsating flows through porous media

Article *in* La Rivista del Nuovo Cimento · November 2014

DOI: 10.1393/ncr/i2014-10106-6

2 authors, including:

J. M. Valverde
Universidad de Sevilla
229 PUBLICATIONS **7,876** CITATIONS

SEE PROFILE

Acoustic streaming in pulsating flows through porous media

Jose Manuel Valverde* and Francisco J. Durán-Olivencia

Faculty of Physics. University of Seville. Avenida Reina Mercedes s/n, 41012 Seville, Spain

(Dated: October 22, 2014)

Abstract

When a body immersed in a viscous fluid is subjected to a sound wave (or, equivalently, the body oscillates in a fluid otherwise at rest) a rotational fluid stream develops across a boundary layer nearby the fluid-body interphase. This so-called acoustic streaming phenomenon is responsible for a notable enhancement of heat, mass and momentum transfer and takes place in processes involving two phases subjected to relative oscillations. Understanding the fundamental mechanisms governing acoustic streaming in two-phase flows is of great interest for a wide range of applications such as sonoprocessed fluidized bed reactors, thermoacoustic refrigerators/engines, pulsatile flows through veins/arteries, hemodialysis devices, pipes in off-shore platforms, offshore piers, vibrating structures in the power-generating industry, lab-on-a-chip microfluidics and microgravity acoustic levitation, and solar thermal collectors to name a few. The aim of engineering studies on this vast diversity of systems is oriented towards maximizing the efficiency of each particular process. Even though practical problems are usually approached from disparate disciplines without any apparent linkage, the behavior of these systems is influenced by the same underlying physics. In general, acoustic streaming occurs within the interstices of porous media and usually in the presence of externally imposed steady fluid flows, which gives rise to important effects arising from the interference between viscous boundary layers developed around nearby solid surfaces and the nonlinear coupling between the oscillating and steady flows. This manuscript is mainly devoted to highlighting the fundamental physics behind acoustic streaming in porous media in order to provide a simple instrument to assess the relevance of this phenomenon in each particular application. The exact microscopic Navier-Stokes equations will be numerically solved for a simplified 2D system consisting of a regular array of oscillating cylinders subjected to an externally imposed steady flow. Results on the pressure drop associated with viscous losses will be compared with predictions from a simple analytical model in which the interaction between the streaming flows developed around the particles and between the oscillating and steady flows are neglected.

* Corresponding author at: Faculty of Physics, Avda. Reina Mercedes s/n, 41012 Seville (Spain). Phone no. +34 954550960. Fax no. +34 954239434. Email: jmillan@us.es

I. INTRODUCTION

The incidence of a sound wave upon a body immersed in a viscous fluid gives rise to the development of a rotational flow field in the close vicinity of the fluid-body interface [1]. This so-called *Acoustic streaming* phenomenon is equivalently retrieved from the oscillations of a body immersed in a viscous fluid otherwise at rest (see Fig. 1). Acoustic streaming may lead to a notable enhancement of the transfer of heat, mass and momentum between the fluid and the body [2], which has a great influence on physicochemical processes occurring in a wide diversity of systems such as sonoprocessed gas-fluidized bed reactors [3–5], thermoacoustic refrigerators/engines [6], reactor fuel rods [7], regeneration/evaporation of liquid drops [8], micron-scale lab-on-a-chip liquid/particle mixing [9] and solar thermal collectors [10] among many others. Generally, the enhancement of heat/mass transfer is useful to intensify these processes. On the other hand, the enhancement of momentum transfer leads to additional energy loss by viscous dissipation, which may be an important source of inefficiency in some cases as in thermoacoustic devices [11] or cycling [12] where it should be minimized.

The motion of a viscous fluid is generally governed by the Navier-Stokes conservation of momentum equation

$$\frac{\partial \mathbf{u}}{\partial t} + (\mathbf{u}\cdot\nabla)\mathbf{u} = -\frac{1}{\rho}\nabla p + \nu\nabla^2\mathbf{u} \tag{1}$$

where p is the fluid pressure, μ is the dynamic fluid viscosity, ρ is the fluid density and $\nu \equiv \mu/\rho$ is the kinematic viscosity. The solution of Eq. 1 for the fluid flow around a solid bounded by an infinite plane and oscillating in the direction of the plane with an angular frequency $\omega = 2\pi f$ is characterized by a rotational fluid flow field damped exponentially with increasing distance from the fluid-solid boundary [13]. The damping depth at which the rotational flow decays by a factor $1/e$ is given by

$$\delta_\nu = \sqrt{\frac{2\nu}{\omega}} \tag{2}$$

which is the so-called Stokes/viscous boundary layer thickness or penetration depth. In the case of a body of arbitrary shape, different types of flow regime may be identified depending on the ratio of the typical body size R to the thickness of the viscous boundary layer (R/δ_ν) and the ratio of the oscillation amplitude to the body size (ξ_1/R), which determine the relative influence of the terms intervening in Eq. 1 [13–15].

$$\left|\frac{\partial \mathbf{u}}{\partial t}\right| \sim \omega^2 \xi_1 \tag{3}$$

$$|(\mathbf{u}\times\nabla)\mathbf{u}| \sim \frac{\omega^2 \xi_1^2}{R} \tag{4}$$

$$\left|\nu\nabla^2\mathbf{u}\right| \sim \nu\frac{\omega\xi_1}{R^2} \tag{5}$$

The non-linear term $|(\mathbf{u}\times\nabla)\mathbf{u}|$ is negligible as compared to the viscous term $\left|\nu\nabla^2\mathbf{u}\right|$ if the Reynolds number Re_1

$$Re_1 = \frac{v_1 R}{\nu} \sim \frac{\xi_1}{R}\left(\frac{R}{\delta_\nu}\right)^2 \tag{6}$$

is small. If the non-linear term is, under this condition, dismissed the fluid flow field turns out to be rotational in a certain layer of thickness δ_ν (Schlichting or inner streaming) changing to potential (irrotational) as the distance from the body increases [13]. In the limit $R >> \delta_\nu$ and for relatively small amplitudes of oscillation ($\xi_1 << R$), the streaming flow remains attached to the body and laminar since the oscillatory fluid particles transverse short distances relative to the solid. Then, the term $|(\mathbf{u}\times\nabla)\mathbf{u}|$ is negligible as compared to $\left|\frac{\partial \mathbf{u}}{\partial t}\right|$ and may be dismissed in Eq. 1 even in the case that Re_1 is not small. When the amplitudes of oscillations are large, inertial stresses become important leading to nonlinear phenomena such as boundary layer separation and wake flows (see Fig. 2). In the limit $R << \delta_\nu$ the term $\left|\frac{\partial \mathbf{u}}{\partial t}\right|$ in Eq. 1 is much smaller than $\left|\nu\nabla^2\mathbf{u}\right|$. This means that the fluid flow field is approximately steady as if it were moving with respect to the solid with a instantaneous velocity equal to the velocity of the solid at any given instant. Then, inertial stresses are much smaller than viscous stresses and the fluid flow can be regarded as steady at any given instant with negligible vorticity for small amplitude oscillations. In the intermediate regime ($R/\delta_\nu \sim \xi_1/R \sim 1$) a prevailing single mechanism cannot be identified.

Using the slip velocity at the edge of the viscous boundary layer as a boundary condition, the development of recirculation flow patterns away from the viscous boundary layer is predicted (Rayleigh/outer streaming) [16]. The size of these outer vortices scales with the size of the confinement as observed experimentally [17].

Intensification of the fluid-solid heat/mass transfer depends basically on the value reached by the streaming Reynolds number $Re_s \equiv v_s R/\nu$. Here v_s is a typical value of the gas velocity at the edge of the viscous boundary layer (slip velocity), which is typically estimated as $v_s \sim v_1^2/\omega R$ [2, 18, 19], thus

$$Re_s \equiv \frac{v_s R}{\nu} \simeq \left(\frac{\xi_1}{\delta_\nu}\right)^2 \tag{7}$$

The cycle-average Nusselt number Nu, representing the ratio of convective (as due to gas-solid relative motion) to conductive-heat/diffusive-mass transfer normal to the gas-solid boundary, is shown to scale proportionally to $Re_s^{1/2}$ for a wide variety of geometries and conditions [2, 18, 20–22]

$$Nu \sim Re_s^{1/2} \sim \frac{\xi_1}{\delta_\nu} \tag{8}$$

Usually, sound intensity is expressed in decibels as

$$SIL = 10\log_{10}\frac{I_1}{I_{ref}} \tag{9}$$

where $I_{ref} = 10^{-12}$ W/m^2 is a reference intensity (the threshold intensity for human hearing) and

$$I_1 = \frac{1}{2}\rho v_1^2 c \quad (\text{W/m}^2) \tag{10}$$

represents the average rate of energy transmission by the traveling wave per unit area in the direction of sound propagation, being c the wave propagation velocity. Since $SIL = 10\log_{10}(\rho c \nu \omega Re_s/2I_{ref})$, a straightforward method to intensify heat/mass transfer based processes is to apply a high intensity acoustic field. The minimum level of sound intensity to promote a diversity of processes by means of high intensity acoustic fields is found to be around 130 dB [4]. At ambient temperature, this SIL value yields a Mach number $M = v_1/c \simeq 6\times10^{-4}$. Generally, the threshold value of the Mach number for the generation of nonlinear effects in liquid-solid systems is around 10^{-4} whereas for gas-solid systems, it is is about one order of magnitude greater. Process intensification by sound waves is thus strongly linked to nonlinearities in the fluid flow field, which will also cause an intensification of momentum transfer. This will be the main subject of the present work and will be considered in further detail in section IV.

II. ACOUSTIC STREAMING IN SONOPROCESSED GAS-FLUIDIZED BED REACTORS

Sonoprocessing is especially useful for intensifying gas-solid reactions in fluidized beds that may be limited in practice by inefficient heat and mass transfer as seen, for example, when high intensity acoustic waves are applied to coal combustors [20, 23] and CaO carbonators [5, 24]

based on gas-fluidized beds operated at high temperature. In gas-fluidized beds a stream of gas is passed through a bed of solid particles at a rate sufficiently high for the overall drag force to balance the bed weight per unit area. Even though fluidized beds may exhibit a wide diversity of dynamic regimes depending on the gas flow rate, particle and gas physical properties, temperature, fluidization assistance methods (mechanical agitation, secondary high velocity flows, electric/magnetic fields, etc.) and bed geometry [25], a number of main issues render the analysis of acoustic streaming in these multiparticle gas-solid systems quite complex. To begin with, particles with low inertia will be entrained in the oscillating flow field of the acoustic wave. For these particles, relative gas-solid oscillations (and therefore acoustic streaming) will be prevented. Entrainment of particles in the acoustic field would occur if the frictional force exerted on the particles by gas oscillations becomes large as compared with particle inertia, i.e. $\mu d_p >> m_p \omega$, where d_p is particle size, $m_p = (1/6)\pi d_p^3 \rho_p$ is particle mass and ρ_p is particle density. As a rule of thumb, entrainment is significant for particles of size lower than 100 μm when subjected to low frequency acoustic fields ($f < 1$ kHz) [26]. Higher frequency acoustic fields are thus necessary to provoke acoustic streaming in fluidized beds of particles smaller than about 100 μm [20, 23]. On the other hand, fine powders (of size below $\sim$50 μm belonging to the Geldart C category [27]) display a strongly heterogeneous fluidization behavior due to the intense attractive forces between the particles as compared to their weight [25, 28]. Strong aggregates and enduring gas channels are commonly developed in fluidized beds of fine particles through which the gas flow finds a bypass, which severely impairs the heat/mass transfer efficiency. Thus, even though acoustic streaming is nullified in these fluidized beds by the entrainment of fine particles in the sound wave, the strong agitation provided by the sound wave helps in destabilizing gas channels and breaking aggregates, which helps to promote gas-solid processes carried out in fluidized beds of fine and ultrafine powders [24, 29–32].

Acoustic streaming will play a role in the case of fluidized beds of particles with sufficiently large inertia in order to not be entrained in the acoustic field (typically in the size range between 100 μm and 1 mm for low frequency acoustic fields). Theoretical studies on acoustic streaming reported in specialized acoustics journals are primarily focused on the limit $\delta_\nu << R$ since in most practical situations considered the sound wave interacts with large macroscopic objects at rest [33]. However, particles in sonoprocessed fluidized beds are small and typically subjected to low frequency sound waves ($f < 1$ kHz) of high intensity (SIL$\gtrsim$120 dB). By taking into account a single particle, acoustic streaming would be characterized in this range of parameters by

relatively large values of the thickness of the viscous boundary layer ($R \lesssim \delta_\nu$), large oscillation amplitudes ($\xi_1 \gtrsim R$) and large values of the streaming Reynolds numbers ($Re_s = (\xi_1/\delta_\nu)^2 \gtrsim 1$, which leads to the development of vortical flows extending to distances well beyond the size of the particles with intense heat/mass transfer at the gas-solid interphase [26]. Thus, and despite of the low to moderate values of the Reynolds number based on the oscillation velocity amplitude $Re_1 = v_1 R/\nu = Re_s R/\xi_1 \lesssim 1$, many processes in gas-fluidized beds are seen to be promoted by the application of high intensity acoustic fields [3–5, 24]

Important issues concerning acoustic streaming in fluidized beds regard the interference between the viscous boundary layers developed around nearby particles particles and the coupling between the main and oscillating gas flows. Since the interparticle separation distance in fluidized beds is typically comparable to particle size [25], the vortical flows between neighboring particles will be likely to interfere. On the other hand, external flows of high intensity will be expected to have a noticeable effect on acoustic streaming. Figure 1 illustrates the deformation suffered by the viscous boundary layer developed around an oscillating cylinder subjected to a steady gas flow and for similar values of the oscillation velocity v_1 and the superficial gas velocity of the steady flow v_g. For sufficiently high values of v_g as compared to v_1, the steady flow might blow away the streaming vortices as observed for liquid droplets levitated by an acoustic field and simultaneously subjected to a steady gas flow [8]. In a gas fluidized bed, the ratio of the oscillation velocity amplitude v_1 and the steady gas flow velocity v_g will thus play an important role in acoustic streaming. In principle, it might be thought that acoustic streaming would be swept away by the external flow in the case of large gas velocities such as those typical of fast fluidized beds employed in many industrial processes relying on circulating fluidized bed (CFB) reactors [34]. However, particles in CFBs become typically entrained in the gas stream. Thus, the relative velocity between the fluidizing gas and the particles would be much lower than the fluidizing gas velocity [35]. In this case, the relative velocity between the superposed acoustic wave oscillations and the particles might be relevant leading to acoustic streaming. This is demonstrated by the intensification of combustion of coal particles fluidized by large gas velocities (of the order of m/s) in fast fluidized beds as due to a significant enhancement of heat/mass transfer when subjected to high intensity sound waves [23].

III. ACOUSTIC STREAMING IN THERMOACOUSTIC DEVICES

Even though fluid compressibility is a necessary condition for the propagation of acoustic waves, most of studies on acoustic streaming consider the fluid as incompressible, which can be a good approximation only when the wavelength λ of the acoustic fields is much larger than the typical size of the solid [36] (this condition is obviously met in the case of a body undergoing oscillations in a viscous fluid). Otherwise, fluid compressibility leads generally to larger streaming velocities outside the viscous boundary layer [37]. Moreover, the compressibility of the fluid gives rise to a gradient in the heat transfer to the solid [36, 38], which is at the basis of refrigerators and engines employed in a rapidly growing field of applications [6].

In the so-called thermoacoustic refrigerators, heat is transferred between the sound wave and a thermally insulating porous solid (stack) as the gas compress and expands moving reciprocally and transferring heat to an end of the solid while taking it from the other. Conversely, sound waves (which may be converted to electric power using a transducer) are generated in thermoacoustic engines by a temperature gradient existing across the porous solid [6]. The linear dimension that characterizes the heat transfer by diffusion between the working gas and the solid is the thermal penetration depth $\delta_\chi = (2\chi/\omega)^{1/2}$, where χ is the fluid's thermal diffusion coefficient. This is the typical distance over which heat can diffuse during a period of the acoustic oscillation i.e. the thickness of the region close to the solid boundary in which heat transfer effectively occurs with the gas. Thermoacoustic streaming will be basically determined by the viscous and thermal Lautrec numbers defined as the ratio of the typical pore size D_h (hydraulic diameter) to the viscous and thermal penetration depths, respectively ($L_\nu = D_h/\delta_\nu$ and $L_\chi = D_h/\delta_\chi$) [6, 39]. For most gases the viscous and thermal penetration depths are similar, thus $L_\nu \simeq L_\chi$. If the typical pore size were substantially greater than δ_χ, the internal solid boundaries would respond independently [40]. However, stacks in thermoacoustic devices typically have pores of size comparable to δ_χ in order to maximize the exchange of heat with the working gas [11]. Moreover, the displacement amplitude of the sound wave is often very large as compared with the viscous penetration depth ($\xi_1 >> \delta_\nu$) in contrast with common situations considered by audio-acoustics. In the case of thermoacoustic systems operated by a standing wave, optimum energy conversion is empirically seen to be achieved for $L_\chi^2 \approx \pi$, which suggests that the efficiency of the device would be significantly improved by employing stacks of varying pore size taking into account the change of the fluid's thermal diffusion coefficient with temperature. However, experimental results show

otherwise presumably due to viscous losses associated to inner streaming [41].

Generally, acoustic streaming leads to harmful effects in thermoacoustic devices preventing them for reaching their full potential efficiency according to the laws of thermodynamics [42, 43]. For example, large-scale convection within the device caused by outer (Rayleigh) streaming may transport heat from its hot to the cold end and rest efficiency to the device at high sound intensities, which is mitigated in practice by tapering the tube [11, 43]. Complex interactions between outer streaming vortical flows developed at the edge of a parallel-plate stack have been experimentally observed by means of particle image velocimetry (PIV) [44, 45] and inferred from numerical simulations [46]. On the other hand, very little is known about inner streaming occurring within the pores of the regenerator or stack, of which experimental evidences seriously affecting the functioning of these devices do exist [11]. Since the viscous penetration depth can be of the order of the typical pore size, the interaction between the vortical flows developed within the pores of the solid would have an important effect on the performance of thermoacoustic devices which remains unexplored yet [43, 47].

An alternative thermoacoustic refrigeration concept is based on the external application of a steady gas flow through the stack in the direction from the hot end to the cold end which is superposed to the oscillating sound wave [43, 48, 49]. In these devices the process gas serves itself as the cyclic thermodynamic working fluid. Since the gas flow to be cooled is used as part of the mechanism, the substantial efficiency penalty imposed by the employ of heat exchangers would be overcome while the acoustic power needed to drive the refrigerator is not increased. Similarly, open cycle traveling wave thermoacoustic engines involve an externally imposed gas flow that travels from the hot to the cold end in the direction opposite to the acoustic wave resulting in the amplification of the traveling acoustic wave [47]. These novel thermoacoustic refrigerators/engines closely resemble sonoprocessed fluidized bed reactors. In both systems a steady and oscillatory fluid flows are superposed within the porous medium. The superposition of steady and oscillatory flows is usually referred to as pulsatile flow [50] and takes place in a wide number of systems other than thermoacoustic devices and sonoprocessed beds such as blood circulation through veins and arteries [51], hemodialysis [52], off-shore platforms [53] and solar thermal collectors [10]. The functioning of these vast class of systems will be determined to a certain extent by the effect of acoustic streaming on the transfer of momentum, which will be the focus of the rest of the manuscript.

IV. TRANSFER OF MOMENTUM IN OSCILLATORY AND PULSATILE FLOWS

The study of momentum transfer through a porous solid subjected to an oscillatory flow is useful for searching of optimum system configurations and physical parameters that provide minimum viscous losses associated to acoustic streaming in each particular application [54–58]. Empirical results reported in the context of thermoacoustic refrigerators and using diverse types of porous media show that viscous friction is governed by the dimensionless oscillation amplitude ξ_1/D_h and the viscous Lautrec number $L_\nu = D_h/\delta_\nu$ [54, 56, 58]. Nonetheless, the fitting parameters in empirical equations usually show a strong dependence on the porosity and internal structure of the porous solid as inferred from measurements on diverse media such as woven wire screens [54, 56], metal mesh screens and felts [55] and open-cell foams [58]. Generally, the cycle-averaged pressure drop through a porous solid as due to an oscillatory flow is found to be several times higher than that due to a steady flow at the same Reynolds numbers based on the cycle-averaged and superficial gas velocities of both flows. Likewise, friction factors are obtained for pulsatile flows through pipes which are notably greater than the expected values for steady flows [50]. Clearly, there is a need of gaining some scientific understanding on the physical mechanism underlying these empirical observations on a wide diversity of systems subjected to oscillatory and pulsatile flows. To this end, we will firstly analyze the results stemming from a simple analytical model based on noninteracting oscillating spheres. Later on, a microscopic numerical approach will be used to further investigate the effects of the interaction between the viscous boundary layers developed around nearby particles as well as the interaction between inner acoustic streaming and an externally imposed steady gas flow.

V. TRANSFER OF MOMENTUM IN OSCILLATORY FLOWS. A SIMPLE ANALYTICAL MODEL

In the limit of either small oscillation displacements ($\xi_1/R < 1$) or small Reynolds number Re_1 (Eq. 6) the non-linear term in Eq. 1 $(\mathbf{u}\times\nabla)\mathbf{u}$ may be neglected and the drag force exerted by a viscous fluid on a solid sphere undergoing relative oscillations at a velocity $v_1(t) = v_1 \sin\omega t$ can be readily calculated as [13, 59]

$$F_1(t) = 6\pi\mu R\left(1+\frac{R}{\delta_\nu}\right)v_1(t) + 3\pi R^2\sqrt{2\mu\rho/\omega}\left(1+\frac{2R}{9\delta_\nu}\right)\frac{dv_1}{dt} = \alpha v_1(t) + \beta\frac{dv_1}{dt} \qquad (11)$$

which converges to the Stokes drag force caused by a steady fluid flow on a sphere ($F_s = 6\pi\mu R v_1$) in the limit $\omega \to 0$ at low Reynolds numbers. As may be seen in Eq. 11, acoustic streaming leads to an increase of the dissipative term of the drag force by a factor $\alpha = 1 + R/\delta_\nu$. The larger the frequency the greater the cycled-averaged (root mean square) dissipated energy per unit time as due to the frictional drag on the surface of the particles $W_1' = \langle F_1 v_1(t) \rangle = (1/2)\alpha v_1^2$. In regards to the inertial term in Eq. 11, it leads to a phase shift between the force and the oscillation velocity (similarly to the phase shift between voltage and current in a conductor carrying alternating current)

$$\varphi = \arctan\left(\omega\beta/\alpha\right) = \arctan\left[\left(\frac{R}{\delta_\nu}\right)\frac{1+2R/9\delta_\nu}{1+R/\delta_\nu}\right] \tag{12}$$

Let us consider a system of solid spheres in a viscous fluid separated by a typical distance d undergoing oscillations. Equation 11 allows us to estimate the cycled-averaged fluid pressure drop per unit length (dp_1^{rms}/dz), which determines the transfer of momentum per unit time and unit volume. Under the assumption that the spheres do not interact it would be

$$\frac{dp_1^{rms}}{dz} = nF_1^{rms} = \frac{3\phi}{4\pi R^3}\left[\alpha^2 + (\omega\beta)^2)\right]^{1/2} u_1^{rms} \tag{13}$$

where $u_1^{rms} = v_1/\sqrt{2}$, n is the number of spheres per unit volume and ϕ is the volume fraction filled by the spheres. On the other hand, the pressure drop of a steady fluid flow passing across a fixed bed of particles can be approximately obtained from the semi-empirical Carman-Kozeny equation [60, 61]

$$\frac{dp_g}{dz} = E\frac{\phi^2}{(1-\phi)^3}\frac{\mu}{d_p^2}v_g \tag{14}$$

where v_g is the superficial fluid velocity, d_p is particle size, and E is an empirical constant basically depending on particle's shape ($E \simeq 180/\Phi_s$, where Φ_s is the sphericity of the particles). Equation 13 was originally derived by modeling a granular bed as a group of capillaries parallel to the direction of flow and of diameter d_p and its validity is restricted to the limit of low Reynolds number based on the gas velocity ($Re_g = v_g R/\nu < 1$).

The relative magnitude of the cycle-averaged pressure drop across a fixed bed of spheres due to an oscillatory flow as compared to that caused by a steady flow can be estimated from Eqs. 13 and 14

$$\frac{dp_1^{rms}}{dp_g} = \frac{(1-\phi)^3}{10\phi}\left[\left(1+\frac{R}{\delta_\nu}\right)^2 + \left(\frac{R}{\delta_\nu}\right)^2\left(1+\frac{2R}{9\delta_\nu}\right)^2\right]^{1/2}\frac{u_1^{rms}}{v_g} \tag{15}$$

which is typically larger than one in accordance to empirical measurements from experiments on oscillatory flows in a diversity of porous solids [54, 56, 58].

In the limits of small particle size and low oscillation frequencies it would be typically $\delta_\nu >> R$. The requirement of low Reynolds numbers (Eq. 6) for Eq. 11 to be valid may be then fulfilled even at large oscillation amplitudes (or, equivalently high sound intensities) as it is usually the case in sonoprocessed beds. On the other hand, the interaction between the viscous boundary layers developed around the particles could be neglected for Eq. 13 to be justifiable only in the limit of very diluted beds ($d >> \delta_\nu >> R \leftrightarrow \phi << 1$). Under this assumption, the ratio of the inertial term to the viscous term in the drag force is $\omega\beta/\alpha \simeq R/\delta_\nu << 1$. Thus, viscous dissipation becomes the dominant mechanism and the pressure drop will oscillate almost in phase with the oscillation velocity ($\varphi \to 0$ in Eq. 12). The ratio of the cycle-averaged pressure drop to the pressure drop due to a steady flow (Eq. 15) is then

$$\frac{dp_1^{rms}}{dp_g} \simeq \frac{(1-\phi)^3}{10\phi}\left(1+\frac{R}{\delta_\nu}\right)\frac{u_1^{rms}}{v_g} \sim \frac{1}{10\phi}\frac{u_1^{rms}}{v_g} \tag{16}$$

For comparable values of oscillating and steady gas velocities ($u_1^{rms} \sim v_g$), and taking into account the limit $\phi << 1$, Eq. 16 predicts larger values of the ratio of the cycled-averaged pressure drop (as due to acoustic streaming) to the pressure drop caused by a steady flow the lower the particle volume fraction.

In fluidized beds and stacks in thermoacoustic devices, the interparticle separation distance is typically of the order of particle size ($d \sim d_p$). Thus, Eq. 13 is strictly admissible only in the limit $\delta_\nu << d \sim R$, which would further require small oscillation displacements ($\xi_1 << R$) for the Reynolds number (Eq. 6) to be small as required to derive Eq. 11. This might be the case of relatively low sound intensities and high frequencies. The ratio of the inertial to the viscous force term is then $\omega\beta/\alpha \simeq (2/9)R/\delta_\nu >> 1$, which means that pressure oscillations lag behind the oscillation velocity by a phase difference close to $\pi/2$ ($\varphi \to \pi/2$ in Eq. 12). The ratio of the cycle-averaged pressure drop to the pressure drop due to a steady flow (Eq. 15) is in this limit

$$\frac{dp_1^{rms}}{dp_g} \simeq \frac{(1-\phi)^3}{45\phi}\left(\frac{R}{\delta_\nu}\right)^2\frac{u_1^{rms}}{v_g} \tag{17}$$

For $u_1^{rms} = v_g$, Eq. 17 predicts that oscillatory flows would give rise to relatively higher pressure drops for $R/\delta_\nu \gtrsim 10$ within the range $\phi \lesssim 0.4$ (typical of fluidized beds [25]). At higher values of ϕ the bed would be close to the packed state ($\phi \simeq 0.56$ in the random loose packing limit of hard spheres [62]) and the interaction between the viscous boundary layer of neighbor particles could not be dismissed. Taking into account the Nusselt number (Eq. 8) for evaluating the intensification of heat/mass transfer and using Eq. 17 for assessing the enhancement of momentum transfer, it may be estimated that by minimizing the ratio

$$\varsigma \equiv \frac{dp_1^{rms}/dp_g}{Nu} \simeq \left(\frac{R}{\delta_\nu}\right)\frac{\omega R}{v_g} \tag{18}$$

the heat/mass transfer would be maximized while viscous losses associated to acoustic streaming are kept relatively low. At a given gas velocity, this would be favored by low frequencies and small particle sizes even though in these limits particles could be entrained in the sound wave if they are free to move as in fluidized beds. For not entrainment ($\omega R^2 >> \mu/\rho_p$) and $\varsigma << 1$ to occur simultaneously, the particle Reynolds number Re_p based on the gas velocity and viscous penetration depth

$$Re_p \equiv \frac{\rho_p v_g \delta_\nu}{\mu} \tag{19}$$

should be large, which is easily met at low frequencies ($f < 1$ kHz) for typical values of gases viscosity and solids density. The condition $d >> \delta_\nu$ to neglect the interaction between boundary layers is however more restrictive. Performing a more rigorous analysis of the general case of pulsatile flows where steady and oscillatory flows of relatively high intensity are superposed and the thickness of the viscous boundary layer may be of the order of the interparticle distance requires a numerical approach, which will be the subject of the rest of the paper.

VI. TRANSFER OF MOMENTUM IN PULSATILE FLOWS. NUMERICAL APPROACHES

A. Macroscopic two-phase models

Heat, mass and momentum transfer in porous media subjected to pulsatile flows have been usually analyzed from the numerical solution of volume averaged macroscopic equations of conservation for the fluid and porous solid phases [10, 63–65]. A goal of these numerical studies is to search for an optimum structure leading to a significant enhancement of heat/mass transfer

while at the same time energy loss due to momentum transfer is minimized. Commonly used governing parameters are the viscous Lautrec number based on the pipe diameter D (D/δ_ν so-called dimensionless frequency parameter) and the ratio of the cycled averaged oscillation velocity to the steady flow velocity (u_1^{rms}/v_g so-called velocity amplitude ratio). Macroscopic two-phase models are based on averaging the microscopic exact equations over a finite size volume that contains both phases since it is generally an impossible task to solve the exact conservation equations for real geometries in porous solids. The averaging volume in macroscopic models is much smaller than the system size but large compared to the typical size of the interfacial micro-structures. This approach is useful to analyze the behavior of complex porous solids such as metal-foams, whose rheological response if characterized by constitutive phenomenological relations [10, 63–65]. On the other hand, volume averaging precludes the analysis of inherently microscopic phenomena occurring at the pore scale such as inner acoustic streaming that ultimately determine the various constitutive relations empirically inferred for the drag and heat/mass transfer coefficients. Usually there exists considerable uncertainty in the modeling of the interfacial transfer terms and effective properties of porous media, which are commonly considered as empirical constants even though they would likely show spatiotemporal variations such as a non-negligible dependence on the oscillation frequency. In our work we have adopted an alternative approach by solving the microscopic momentum and mass conservation equations (exact equations without phenomenological parameters) at the expense of considering an over-simplified system.

B. Microscopic approaches

While realistic porous solids used in applications entail far more complicated structures, the main aim of our study is to get a grip on the fundamental role of inner acoustic streaming as a driving mechanism. To this end we will consider a simple 2D system consisting of an oscillating array of circular cylinders contained between two parallel plates and subjected to a steady gas flow. Nonetheless, there exist still a wide number of engineering applications in which the hydrodynamic interaction of a multiple array of oscillating cylinders is particularly relevant such as reactor fuel rods, heat exchanger tubes, offshore piers and other types of structures [53, 66, 67]. The turbulence of axial flows along bundles of reactor fuel rods cause small-amplitude random vibrations, which leads to an enhancement of viscous friction [7]. A number of works have been focused on this problem recently incorporating 2D arbitrary Lagrangian Eulerian (ALE) finite

element analysis to compute the hydrodynamic coupling effects in the limit of small amplitude oscillations [68]. The effect of hydrodynamic interactions among transversely oscillating cylinders in an unbounded mass of viscous incompressible fluid was already revealed in an early theoretical study [69]. By means of a transformation method, hydrodynamic forces could be decomposed in a self-excited part and a mutually excited part, each one containing an inertial term and a viscous dissipative term. The latter one predominated in the low-frequency regime for which the viscous boundary layer around each cylinder was thick ($R/\delta_\nu < 1$). If the spacing between cylinders d was smaller than δ_ν, the boundary layers around the cylinders overlapped. The cylinders appeared then as a nonporous solid embedded in a boundary layer surrounding the whole array. In the high-frequency limit ($R > \delta_\nu$) and if $d > \delta_\nu$, the flow field could be described as irrotational in between effective cylinders of size enlarged by the viscous boundary layer wherein the rotational flow remained confined (the interaction between the irrotational and rotational flows was week). A system of multiple oscillating cylinders operating in this regime has been proposed very recently for transporting microparticles in *lab on a chip* applications that may be trapped in the streaming cell around selected cylinders depending on its oscillation parameters [15]. On the other hand, if $d < \delta_\nu$ and for high frequencies ($R/\delta_\nu > 1$), the force coefficients were relevantly affected by the complicated interactions between the viscous boundary layers around each cylinder. The streaming interference between nearby cylinders oscillating along the line joining their centers has been analyzed theoretically by Coenen and Riley [70] resulting in the development of jets perpendicular to the direction of oscillation. Yet, these studies are restricted to the limit of small oscillation amplitude ($\xi_1/R << 1$) as corresponds to conditions in practice for heat exchangers and reactor fuel rods. Moreover, the fluid motion is assumed to be due entirely to the oscillations of the cylinders, which allows linearizing the momentum conservation equation and neglecting the convective term. Otherwise, the vortical flow may detach from the fluid-solid boundary and propagate into the fluid. This is likely the case of thermoacoustic devices and sonoprocessed beds where the amplitude of the oscillations may be typically larger than the pore size and the externally imposed gas flow will give rise to further convective effects. The influence of these non-linear phenomena can be only considered by numerically solving the microscopic Navier-Stokes equations.

VII. NUMERICAL SCHEME AND SOLUTION METHOD

Figure 3 shows a schematic representation of the physical system used for numerical calculations in our work. A solidary square array of 17×33 infinite circular cylinders of radius $R = 200$ μm is placed between two solid walls. The cylinders are vertically oscillated with a velocity $v(t) = v_1 \sin(\omega t)$ and subjected to an externally imposed gas flow of superficial velocity v_g.

The governing equations for an unsteady compressible Newtonian flow can be written as follows [13][71],

Mass Conservation :

$$\frac{\partial \rho}{\partial t} + \nabla \cdot (\rho \mathbf{u}) = 0, \tag{20}$$

Momentum Conservation (Eq. 1)

$$\rho \frac{\partial \mathbf{u}}{\partial t} + \rho \left(\mathbf{u} \cdot \nabla\right) \mathbf{u} = \nabla \cdot \left[-p\mathbf{I} + \mu \left(\nabla \mathbf{u} + \left(\nabla \mathbf{u}\right)^{\mathrm{T}} \right) - \frac{2}{3} \mu \left(\nabla \cdot \mathbf{u}\right) \mathbf{I} \right], \tag{21}$$

where $\mathbf{u}$ is the fluid velocity vector. The oscillating boundary condition

$$\mathbf{u}|_{\Gamma_p} = \mathbf{v}_1 \sin(\omega t), \tag{22}$$

is imposed on the particles' surface. In regards to the walls of the container, the slip condition

$$\mathbf{u} \cdot \mathbf{n}|_{\Gamma_{wall}} = 0, \tag{23}$$

is considered, where $\mathbf{n}$ is the unitary vector perpendicular to the boundary. Equation (23) establishes implicitly that there will not be viscous effects at the slip wall where no boundary layer will develop therefore. This may be justified provided that the main role of the boundary is to prevent the fluid from leaving the domain, which is a reasonable approximation in the case of a large number of particles since most of viscous effects will occur at particles' surface. Finally, inlet and outlet boundary conditions

$$\mathbf{u} \cdot \mathbf{n}|_{\Gamma_{inlet}} = \mathbf{u} \cdot \mathbf{n}|_{\Gamma_{outlet}} = v_g. \tag{24}$$

are imposed in order to match the fluid velocity at the boundaries to the velocity of the externally imposed gas flow.

Equations 20 and 21 have been solved by means of the Finite Element Method (FEM), which reduces the original partial differential equation system to a set of algebraic equations. In a standard FEM formulation (Bubnov-Galerkin), the weighting functions used in the weighted residual method are identical to those used for interpolating inside each one of the elements. However, The Navier-Stokes conservation of momentum equation (NSE) is highly nonlinear due to the presence of the convective term $\mathbf{u}\cdot\nabla\mathbf{u}$. In the case of convection dominant problems, and especially in the presence of discontinuities, a standard FEM formulation may lead to non-negligible numerical oscillations, which are the source of inaccuracy and instability. Following the argument of Donea and Huerta [72], a detailed analysis on interior node equation reveals that convection related instabilities arise as a consequence of the symmetry of the weighting functions. In order to avoid these instabilities, two stabilization terms can be added to the residual equation in accordance with a stream upwind procedure. Further details on this methodology used in our work, known as Stream Upwind Petrov-Galerkin (SUPG), are given in the appendix.

Unless otherwise stated, the physical parameters used for the numerical calculations are:

Name	Value	Description
h	4 cm	height cell
W	2 cm	width cell
R	200 μm	cylinder radius
d	4R	gap between neighbor cylinders
c	346 m·s^{-1}	speed of sound (air)
μ	$1.8\cdot10^{-5}$ Pa·s	dynamic viscosity
ρ	1.2 kg·m^{-3}	gas density
f	[25,50,75,100,150,300,500]	frequency range
SIL	[120,125,130,135,140]	sound intensity level range
I_{ref}	10^{-12} W·m^{-2}	standard reference sound intensity
T	298 K	gas temperature
v_g	[0.1,0.3,0.5,0.7,0.9]	inlet gas velocity range

In regards to fluid properties, they have been chosen as those of air at ambient conditions. The effect of operating at high temperatures will be discussed in section VIII B. SIL values are in the

range 120 - 140 dB. The effect of further increasing the sound intensity will be analyzed in section VIII A.

The problem of a bed of particles subjected to an acoustic wave (of very large wave length as compared to system size) and that of a pulsatile flow through a porous bed can be considered from the analysis of the same numerical scheme. In the case of a sonoprocessed bed, the sound intensity level (SIL) is related to the oscillation velocity amplitude v_1 by means of Eqs. 9 and 10. An additional issue with sonoprocessed beds that will not be taken into account in our study is attenuation of the acoustic wave (see [26] for further discussion). In general, the main source of sound energy damping in the range of sonic frequencies stems from energy losses due to viscous friction and thermal conduction on the surface of the particles. For particles of size of the order of hundreds of microns, SIL values may decay by 10 dB typically over distances of a few centimeters depending on the particle volume fraction, which corresponds to a relative decay of the oscillation velocity amplitude by a factor of about two. A further significant attenuation of sound intensity might still occur in large-scale applications due to the divergence of the acoustic wave, which may be overcome by placing an array of sound generators capable of reproducing a plane-wave acoustic field without a significant evanescence for low sonic frequencies [73]. Incorporating sound attenuation into the numerical scheme of our work will be the subject of a separate work.

VIII. NUMERICAL RESULTS AND DISCUSSION

Figure 4 shows curve examples of the gas pressure drop (cross-sectional averaged value) across the array of cylinders ($\Delta p(t)$) as a function of time t for different values of the acoustic wave intensity (SIL), oscillation frequency (f), and external gas flow velocity (v_g). As may be seen, the acoustic wave gives rise to an oscillatory component $\Delta p_1 \sin(\omega t + \varphi)$ which adds up to a steady pressure drop term Δp_g as reported in experimental studies [54, 56, 58]

$$\Delta p(t) = \Delta p_g + \Delta p_1 \sin(\omega t + \varphi) \tag{25}$$

Generally, we observe that the amplitude of the oscillatory term Δp_1 increases with the oscillation velocity amplitude v_1 as might be expected. Figure 5 shows $\Delta p(t)$ curves obtained for given values of v_g and v_1 and for different oscillation frequencies illustrating the phase shift φ between the oscillatory pressure drop and the oscillation velocity, which increases with the oscillation frequency in qualitative agreement with the predicted result from Eq. 12.

Figure 6 is a 3D plot of the numerical results obtained for the ratio $\Delta p_{rms}/\Delta p_g$ (where $\Delta p_{rms} = \Delta p_1/\sqrt{2}$) as a function of the oscillation frequency ($f \in$25 - 500 Hz) and SIL value (SIL $\in$ 120 - 140 dB $\leftrightarrow$ $v_1 \in 0.07 - 0.7$ m/s) when the external gas flow velocity ($v_g = 0.1$ m/s) is similar or below the oscillation velocity amplitude ($v_1/v_g \in 0.7 - 7$). In the range of frequencies tested, the distance between closest neighbors d is larger than the thickness of the viscous boundary layer ($d/\delta_v \in 2 - 8$), thus the interference between the boundary layers developed around nearby cylinders would be expected not to be relevant. Contour lines have been plotted in Fig. 6 onto the 3D surface along which the ratio $\frac{\xi_1}{\delta_v}$ (Nusselt number, Eq. 8) takes constant values, which vary between 0.5 and 4. Nusselt numbers above one would indicate an enhancement of mass/heat transfer associated to acoustic streaming [2, 18, 20–22]. In regards to pressure drop, Fig. 6 shows that the oscillatory pressure drop is enhanced as the SIL level and/or the oscillation frequency are increased in qualitative agreement with Eq. 15. In the range of frequencies and SIL values tested, the results obtained are in the range between $\Delta p_{rms}/\Delta p_g \simeq 2$ for the lowest frequency and SIL values considered (25 Hz, 120 dB) and $\Delta p_{rms}/\Delta p_g \simeq 24$ for the highest frequency and SIL values SIL (500 Hz, 140 dB).

The theoretical prediction by Eq. 15 and numerical results obtained on $\Delta p_{rms}/\Delta p_g$ are jointly plotted in Fig. 7. As may be seen, for the lowest value of v_g ($v_g = 0.1$ m/s), there is a good agreement between the numerical results and theoretical predictions in spite of the simplicity of the analytical model and the 2D limitation of the numerical calculations. As a matter of fact, Eq. 15 was derived from a model based upon a system of ideally noninteracting spheres subjected to a purely oscillatory flow. Therefore, it may be argued that acoustic streaming developed on each individual particle can be just linearly superposed to the external gas flow as long as the external gas velocity is not large ($v_1/v_g > 1$) and the viscous boundary layers remain attached to each particle ($d/\delta_v > 2$). Numerical and theoretical results are plotted in Figs. 7b and 7c for increasing values of the external gas flow velocity ($v_g = 0.5$ m/s and 0.9 m/s, respectively), which causes the ratio v_1/v_g to decrease below one. As can be observed, the ratio $\Delta p_{rms}/\Delta p_g$ is then considerably decreased and becomes smaller than one for $v_g = 0.9$ m/s ($v_1/v_g \in 0.1 - -0.8$), which suggests that acoustic streaming is prevented by a sufficiently intense external gas flow as seen empirically for the streaming vortices developed around liquid droplets levitated by an acoustic field, which are blown away by an intense steady gas flow [8]. This is clearly observed in Fig. 8, where snapshots are shown illustrating main features of the gas streamlines around the cylinders. Streaming vortices are seen to disappear when the superficial gas velocity v_g is large.

Figure 9 is a plot of the numerically obtained values for φ as a function of frequency f. Predicted curves from Eq. 12 are also shown for comparison. Leaving aside the fact that the theoretical model is built upon spheres whereas the numerical model considers infinite circular cylinders, the generally lower values of φ numerically retrieved as compared to the theoretical predicted values could be attributed to effects arising from the influence of the externally imposed gas flow and the interaction between the viscous boundary layers developed around neighbor particles, which are not taken into account in the simple analytical model (Eq. 12). In agreement with this argument, Fig. 9 shows that the phase shift is further decreased as the external gas velocity v_g is increased and/or the oscillation frequency is decreased (i.e. the viscous boundary layer δ_v is thickened) indicating that in both cases the inertial term in the force exerted by the fluid on the particles due to acoustic inner streaming (which is the source of the phase shift) is somewhat mitigated. Arguably, and in accordance with previously shown results on $\Delta p_{rms}/\Delta p_g$ (Fig. 7), an intense externally imposed gas flow hinders the development of acoustic streaming. On the other hand, lowering the oscillation frequency leads to small values of d/δ_v, which would promote the interference between the boundary layers developed around closest cylinders. In the range of frequencies tested (25–500 Hz), it is $d/\delta_v > 2$. Thus the interference between the boundary layers is expected not to be as relevant as the effect of the external gas flow. Accordingly, we see in Fig. 9 a stronger influence played by the external gas flow on the phase shift as compared with the effect of frequency. Nevertheless, the interference between viscous boundary layers would have an important effect if particles were closer and/or the temperature were increased. This issue will be analyzed in further detail ahead (section VIII B).

A further issue to be investigated is whether the steady component of the pressure drop Δp_g stemming form the numerical calculations adjusts to the pressure drop Δp_g^0 that would be obtained in the only presence of the external gas flow. As seen in Fig. 4, Δp_g does not show a remarkable dependence on the amplitude of oscillations in the range of SIL tested. However, Fig. 10a shows that Δp_g^0 increases at a slightly smaller rate with the gas flow velocity v_g as compared to Δp_g. This observation reproduces qualitatively experimental results reported in for sonoprocessed beds [5] eventually leading to a decrease of the minimum fluidization velocity [29].

The above observations might serve to shed light on some unexplained phenomena such as the decrease of the minimum fluidization velocity in sonoprocessed fluidized beds. Another example is the divergence reported between experimental measurements and theoretical results (derived by neglecting acoustic streaming) on the refrigeration power of thermoacoustic refrigerators with an

externally applied gas flow [48]. In the range of small velocities of the applied gas flow v_g, the refrigeration power of these devices is seen to increase with v_g at a lower rate than predicted from a theoretical model just based on thermoacoustic grounds supplemented by an additional applied flow term [48]. Our numerical results suggest that acoustic streaming might bring about an adverse effect transporting heat between different parts of the stack by convective vortices, which will be intense at large values of the oscillation velocity v_1 as compared to v_g as may be seen in Fig. 8(left). On the other hand, the theoretical prediction converges towards the experimentally measured values as the velocity of the external gas flow is increased [48] indicating that the detrimental effect of streaming on the refrigeration power is diminished as inferred from Fig. 8(right). Mitigating the adverse effect of acoustic streaming would represent an additional advantage of thermoacoustic refrigerators/engines with an externally applied gas flow as compared with conventional closed-off thermoacoustic refrigerators in which streaming will be unavoidably present. According to our study, it might be expected that streaming within the porous solid would be minimized for values of $v_1/v_g < 1$. Promoting heat transfer by acoustic streaming yields however a beneficial effect in other applications as, for example, in sonoprocessed fluidized bed reactors where gas-solid reactions are accelerated [5]. Our results might serve in this case to assess the relative velocity between the gas and the solids v_g that would hinder the desired effect of acoustic streaming for a given sound intensity level. Depending on the fluidization regime, the results would yield the threshold SIL value needed to intensify the process.

A. Effect of high intensity acoustic fields

We have just seen that if interparticle distance is over twice the thickness of the viscous boundary layer ($d/\delta > 2$) vorticity remains constrained to the vicinity of the particles in the range of SIL values between 120 and 140 dB. Let us now look in more detail at the effect of increasing the SIL value and therefore oscillation amplitude ξ_1. Figure 11 shows the evolution of the gas streamlines in the vicinity of the cylinders when the SIL value is increased up to 160 dB ($v_1 \simeq 7$ m/s). Trajectories and velocity of tracers introduced in the external gas flow can be seen in Fig. 11 for SIL=120 dB and SIL=160 dB. At 120 dB, the amplitude of oscillations is small ($\xi_1/d \simeq 0.1$) and since $d/\delta_\nu \simeq 3.7 > 2$ the tracers are seen to follow approximately vertical trajectories determined by the external gas flow. In contrast, tracers are diverted towards tortuous paths and experience large velocity oscillations when the sound intensity is increased up to 160 dB. For such high sound

intensity, the amplitude of oscillations is much larger than the interparticle separation distance ($\xi_1/d \simeq 10$), which leads to an enhancement of long range streaming as seen in Fig. 11. Arguably, this would lead to a marked intensification of heat/mass transfer as observed in sonoprocessed fluidized bed reactors that must be operated at very high sound intensity levels [5] (SIL$>$ 140 dB) even though viscous friction will be also promoted thus increasing the energy demand. It must be warned however that the translation of these results to a 3D system can be affected by boundary effects, whose relevance on the dynamics of fluid-solid 3D systems may differ significantly at large Reynolds numbers [74]. 3D simulations in the cases of very high SIL values should be pursued in future works to further investigate this issue.

B. Effect of high temperatures

We have just seen that the interference between the viscous boundary layers developed around neighbor particles does not perturb significantly the gas streamlines between the cylinders as long as $d/\delta_\nu > 2$. The situation will be different if the interparticle distance is decreased and/or the fluid viscosity and density are changed. The latter case can be usually found in gas-solid fluidized bed reactors operated at high temperature [5]. For example, the dynamic viscosity of air raises up from $1.8{\cdot}10^{-5}$ Pa·s at ambient temperature to $4.8{\cdot}10^{-5}$ Pa·s at 900°C while its density is decreased from 1.2 kg·m^{-3} down to 0.3 kg·m^{-3}. Consequently, the ratio d/δ_ν at $f = 25$ Hz is decreased from 2 at ambient temperature to 0.56, which would expectedly cause a non-negligible interaction between the vortices generated around the cylinders. This is confirmed by inspection of Fig. 12 where it is seen that the gas flow lines are markedly perturbed. Similarly to the situation observed when the sound intensity is increased, the externally imposed flow is constrained to follow tortuous paths with long horizontal trajectories, which would expectedly lead to an increase of the viscous drag. This may be seen in Fig. 13, which shows that the oscillatory component of the pressure drop is markedly enhanced whereas the opposite would have been theoretically predicted from a decrease of R/δ_ν if the interaction between boundary layers were neglected (Eq. 15).

IX. CONCLUSIONS

Acoustic streaming is a widespread phenomenon taking place in any two-phase process subjected to oscillatory flows. In general, oscillations give rise to the development of rotational fluid

flows in the close vicinity of interphases extending to distances of the order of $\delta_\nu = \sqrt{2\nu/\omega}$ being ν the fluid kinematic viscosity and ω the angular oscillation frequency. Acoustic streaming is responsible for the enhancement of heat and mass, which is remarkable in the limit of large Nusselt numbers ($Nu = \xi_1 \delta_\nu$ where ξ_1 is the oscillation amplitude). Acoustic streaming has been usually analyzed in the limits $\delta_\nu << R$ and $\xi_1 << R$, where R is the typical size of the oscillating body in the viscous fluid, since this is the typical situation in common audio acoustics engineering problems. However, acoustic streaming may play a relevant role in processes involving porous media immersed in viscous fluids where the typical size of the constituent particles is small as compared to δ_ν. Two examples with relevant engineering applications reviewed in our work are gas-fluidized bed reactors of small particles subjected to high intensity acoustic waves (sono-processed fluidized beds) and thermoacoustic refrigerators and engines. In both cases, the development of acoustic streaming within interstices may have a significant influence on the process efficiency. In the case of thermoacoustic devices inner acoustic streaming is thought to have a detrimental influence yet unexplored whereas it is otherwise in sonoprocessed beds for which empirical studies show that the enhancement of heat and mass transfer caused by acoustic streaming serve to intensify gas-solid reactions. While the physics of individual solid objects oscillating in a viscous fluid is well understood, a fundamental analysis on the more general case of porous solids is precluded by the complex interaction between the viscous boundary layers developed around nearby interphases. Moreover, an externally imposed steady flow of fluid is usually imposed to the oscillatory flow in many cases (pulsatile flows), which complicates further the situation. Despite of the disparate approaches usually adopted to tackle these problems from diverse disciplines, it is possible to adopt a unifying perspective built on a common underlying physics. To get a grip on the main driving mechanism behind acoustic streaming in pulsatile flows through porous media we have solved the microscopic Navier-Stokes equation for a simplified system consisting of a vertically oscillating solidary array of infinite length and small diameter circular cylinders separated by a distance of the order of their size and subjected to a vertical gas flow. Numerical results on the gas pressure drop across the system have been compared with the predicted results derived from a simple analytical model of noninteracting spheres subjected to an oscillatory flow. A main conclusion from this study is that viscous losses in porous media subjected to pulsatile flows are determined by inner acoustic streaming depending on the extent of the viscous boundary layer δ_ν as compared to the typical pore size d and the ratio of the oscillation velocity amplitude v_1 to the external gas velocity v_g. The interaction between viscous boundary layers developed around nearby particles is

not relevant when $d/\delta_v > 2$. In this limit, the transfer of momentum as due to the oscillatory flow conforms approximately to a simple analytical equation derived from the model on noninteracting particles provided that the external gas flow velocity is below the oscillation velocity amplitude ($v_g < v_1$) and the amplitude of oscillations are not large ($\xi_1 \lesssim d$). On the other hand, acoustic streaming is mitigated for $v_g > v_1$, which results in a relative decrease of the transfer of momentum as caused by acoustic streaming. A close look at the fluid streamlines shows that externally imposed intense gas flows ($v_g < v_1$) blow away the vortical flow in the vicinity of the solids. If the viscous boundary layer extends beyond the interparticle separation ($d/\delta_v < 1$) and/or the intensity of oscillations become large (($\xi_1 >> d$), the external fluid flow is diverted toward tortuous trajectories across the porous solid resulting in a significant increase of viscous drag. Both situations may be achieved for example in sono-processed gas-fluidized beds if the operating temperature is increased (as usually to catalyze gas-solid reactions) and/or the intensity of the acoustic wave is increased typically above 140 dB.

X. ACKNOWLEDGEMENTS

Financial support by the Andalusian Regional Government (Junta de Andalucia, contract FQM-5735) and Spanish Government Agency Ministerio de Ciencia e Innovacion (contracts FIS2011-25161) are acknowledged.

Appendix A: Spatial discretization: Streamline upwind method

The Stream Upwind Petrov-Galerkin (SUPG) methodology is based on the definition of weighting functions such that the upwind node is more heavily weighted than the downwind node [75]. The first stabilization term acts on the residual of the continuity equation while the second one is applied on the residual of the momentum equation. In order to stabilize not only the velocity solution but also the pressure solution, the momentum stabilization term is split into three parts related to convection, viscous drag and pressure. The stabilized formulation implemented based on the numerical scheme proposed by Franca and Frey [76][77] can be summarized by mean of the equations

$$\mathscr{W}_\rho + \sum_{e=1}^{N_e} \int_{\Omega_e} \tau_\rho \mathscr{F}_\rho \mathfrak{p}_\rho d\Omega = 0, \tag{A1a}$$

$$\mathscr{W}_{\mathbf{u}} + \sum_{e=1}^{N_e} \int_{\Omega_e} \tau_{\mathbf{u}} \mathscr{F}_{\mathbf{u}} \mathfrak{p}_{\mathbf{u}} d\Omega = 0. \tag{A1b}$$

where $\mathfrak{p}$ designates the corresponding weighting functions in the stabilization terms

$$\mathfrak{p}_\rho = \nabla \cdot \hat{\mathbf{u}}, \tag{A2a}$$

$$\mathfrak{p}_{\mathbf{u}} = \mathfrak{p}_{\mathbf{u}}|_{\text{convective}} + \mathfrak{p}_{\mathbf{u}}|_{\text{viscous}} + \mathfrak{p}_{\mathbf{u}}|_{\text{pressure,}} \tag{A2b}$$

with

$$\mathfrak{p}_{\mathbf{u}}|_{\text{convective}} = \mathbf{u} \cdot \nabla \hat{\mathbf{u}}, \tag{A3a}$$

$$\mathfrak{p}_{\mathbf{u}}|_{\text{viscous}} = -\frac{2}{\text{Re}} \nabla \cdot \hat{\mathbf{D}}, \tag{A3b}$$

$$\mathfrak{p}_{\mathbf{u}}|_{\text{pressure,}} = \nabla \hat{p}. \tag{A3c}$$

The terms $\mathscr{W}$ and $\mathscr{F}$ are employed to represent the standard weak and strong formulation, respectively. The hat superscript indicates the use of corresponding weighting function, *Re* is the fluid Reynolds number and $\mathbf{D}$ is the strain rate tensor. Finally, the stabilization parameters (τ) are taken according to Wall and Ramm [78].

Appendix B: Time discretization: Generalized-α method

Once spatial discretization is carried out, a nonlinear semi-discrete equation emerges. To solve such equation, the "Generalized-α method" [79] along with a linear predictor are used by means of a Newton-Raphson iterative scheme. The "Generalized-α method" is an implicit single-step time integration scheme based on Newmark approximations in the time domain.

---

[1] Sir James Lighthill. Acoustic streaming. *Journal of Sound and Vibration*, 61(3):391 – 418, 1978.

[2] N. Riley. Steady streaming. *Annu. Rev. Fluid Mech.*, 33:43 65, 2001.

[3] S. V. Komarov. *Advanced Topics in Mass Transfer*, chapter Application of Airborne Sound Waves for Mass Transfer Enhancement, pages 61 – 86. InTech, 2011.

[4] Sergey V. Komarov, Mamoru Kuwabara, and Oleg V. Abramov. High power ultrasonics in pyrometallurgy: Current status and recent development. *ISIJ International*, 45(12):1765 – 1782, 2005.

[5] J.M. Valverde, J. M. P. Ebri, and M. A. S. Quintanilla. Acoustic streaming enhances the multicyclic CO_2 capture of natural limestone at Ca-looping conditions. *Environmental Science & Technology*, 47(16):9538 9544, 2013.

[6] Steven L. Garrett. Resource letter: Ta-1: Thermoacoustic engines and refrigerators. *American Journal of Physics*, 72(1):11–17, 2004.

[7] J.O. Gagnon and M.P. Paidoussis. Fluid coupling characteristics and vibration of cylinder cluster in axial flow. part ii: Experiments. *Journal of Fluids and Structures*, 8(3):293 – 324, 1994.

[8] A. L. Yarin, G. Brenn, O. Kastner, D. Rensink, and C. Tropea. Evaporation of acoustically levitated droplets. *J. Fluid Mech.*, 399:151 – 204, 1999.

[9] Frieder Mugele, Adrian Staicu, Rina Bakker, and Dirk van den Ende. Capillary stokes drift: a new driving mechanism for mixing in ac-electrowetting. *Lab Chip*, 11:2011–2016, 2011.

[10] Po-Chuan Huang, Chih-Cheng Chen, and Hsiu-Ying Hwang. Thermal enhancement in a flat-plate solar water collector by flow pulsation and metal-foam blocks. *International Journal of Heat and Mass Transfer*, 61(0):696 – 720, 2013.

[11] Greg W. Swift. *Thermoacoustics: A Unifying Perspective for Some Engines and Refrigerators*. Acoustical Society of America through the American Institute of Physics, 2002.

[12] T. N. Crouch, D. Burton, N. A. T. Brown, M. C. Thompson, and J. Sheridan. Flow topology in the wake of a cyclist and its effect on aerodynamic drag. *Journal of Fluid Mechanics*, 748:5–35, 6 2014.

[13] L. D. Landau and E. M. Lifshitz. *Course of Theoretical Physics*, chapter Fluid Mechanics. Pergamon Press, New York, 1995.

[14] Chang-Yi Wang. On high-frequency oscillatory viscous flows. *Journal of Fluid Mechanics*, 32:55–68, 1968.

[15] Kwitae Chong, Scott D. Kelly, Stuart Smith, and Jeff D. Eldredge. Inertial particle trapping in viscous streaming. *Physics of Fluids*, 25(3):033602, 2013.

[16] Chun P. Lee and Taylor G. Wang. Outer acoustic streaming. *J. Acoust. Soc. Am.*, 88:2367 2375, 1990.

[17] E. H. Trinh and J. L. Robey. Experimental study of streaming flows associated with ultrasonic levitators. *Phys. Fluids*, 6:3567 – 3579, 1994.

[18] A. Gopinath and A. F. Mills. Convective heat transfer from a sphere due to acoustic streaming. *ASME: J. Heat Transf.*, 115:332 – 341, 1993.

[19] A. Gopinath and H. R. Harder. An experimental study of heat transfer from a cylinder in low-amplitude zero - mean oscillatory flows. *Int. J. Heat Mass Trans.*, 43:505 520, 2000.

[20] S. Yavuzkurt, M. Y. Ha, K. Koopmann, and A. W. Scaroni. A model of the enhancement of coal combustion using high-intensity acoustic fields. *Journal of Energy Resources Technology*, 113(4):277 – 285, 1991.

[21] X. Jia, C. Caroli, and B. Velicky. Heat transfer from a vibrating cylinder. *Int. J. Heat Mass Trans.*, 16:1703 1727, 1973.

[22] E. W. Haddon and N. Riley. The steady streaming induced between oscillating circular cylinders. *Q. J. Mech. Appl. Math.*, 32:265 282, 1979.

[23] S. Yavuzkurt, M. Y. Ha, G. Reethof, G. Koopmann, and A. W. Scaroni. Effect of an acoustic field on the combustion of coal particles in a flat flame burner. *Journal of Energy Resources Technology*, 113(4):286 – 293, 1991.

[24] J. M. Valverde, F. Raganati, M. A. S. Quintanilla, J. M. P. Ebri, P. Ammendola, and R. Chirone. Enhancement of CO_2 capture at Ca-looping conditions by high-intensity acoustic fields. *Applied Energy*, 111:538 549, 2013.

[25] Jose Manuel Valverde. *Fluidization of Fine Powders: Cohesive versus Dynamical Aggregation*, volume 18 of *Particle Technology Series*. Springer, 2013.

[26] Jose Manuel Valverde. Acoustic streaming in gas-fluidized beds of small particles. *Soft Matter*, 9:8792 – 8814, 2013.

[27] D. Geldart. Types of gas fluidization. *Powder Technol.*, 7(5):285–292, 1973.

[28] A. Castellanos, J. M. Valverde, and M. A. S. Quintanilla. Aggregation and sedimentation in gas-fluidized beds of cohesive powders. *Phys. Rev. E.*, 64:041304(1) – 041304(7), 2001.

[29] R. Chirone, L. Massimilla, and S. Russo. Bubble-free fluidization of a cohesive powder in an acoustic field. *Chemical Engineering Science*, 48:41 – 52, 1993.

[30] A. Ajbar, Y. Bakhbakhi, S. Ali, and M. Asif. Fluidization of nano-powders: Effect of sound vibration and pre-mixing with group a particles. *Powder Technol.*, 206(3):327–337, 2011.

[31] P. Ammendola, R. Chirone, and F. Raganati. Effect of mixture composition, nanoparticle density and sound intensity on mixing quality of nanopowders. *Chemical Engineering and Processing: Process Intensification*, 50(8):885 – 891, 2011.

[32] F. Raganati, P. Ammendola, and R. Chirone. CO_2 adsorption on fine activated carbon in a sound assisted fluidized bed: Effect of sound intensity and frequency, CO_2 partial pressure and fluidization velocity. *Applied Energy*, 113:1269 – 1282, 2014.

[33] Bakhtier Farouk, Yiqiang Lin, and Zhiheng Lei. Acoustic wave induced flows and heat transfer in gases and supercritical fluids. In Young I. Cho and George A. Greene, editors, *Advances in Heat Transfer*, volume 42 of *Advances in Heat Transfer*, pages 1 – 136. Elsevier, 2010.

[34] D. Kunii and O. Levenspiel. *Fluidization Engineering*. Butterworth-Heinemann, Boston, 2nd edition, 1991.

[35] J. G. Yates. *Fundamentals of fluidized-bed chemical processes*. Monographs in chemical engineering. Butterworths, London, 1983.

[36] Ashok Gopinath and Eugene H. Trinh. Compressibility effects on steady streaming from a noncompact rigid sphere. *The Journal of the Acoustical Society of America*, 108(4):1514 – 1520, 2000.

[37] Quan Qi. The effect of compressibility on acoustic streaming near a rigid boundary for a plane traveling wave. *The Journal of the Acoustical Society of America*, 94(2):1090 – 1098, 1993.

[38] Ashok Gopinath. Thermoacoustic streaming on a sphere. *Proceedings of the Royal Society of London. Series A: Mathematical, Physical and Engineering Sciences*, 456(2002):2419–2439, 2000.

[39] L. A. Wilen. Measurements of thermoacoustic functions for single pores. *The Journal of the Acoustical Society of America*, 103(3):1406 – 1412, 1998.

[40] John Wheatley and Arthur Cox. Natural engines. *Print edition*, 38(8):50 – 58, 1985.

[41] K. Yanagimoto, S.-i. Sakamoto, K. Kuroda, Y. Nakano, and Y. Watanabe. Improvement of energy conversion efficiency of thermoacoustic engine by a multistage stack with multiple pore radii. In T. Kamakura and N. Sugimoto, editors, *American Institute of Physics Conference Series*, volume 1474 of *American Institute of Physics Conference Series*, pages 279–282, September 2012.

[42] W. Pat Arnott, Henry E. Bass, and Richard Raspet. General formulation of thermoacoustics for stacks having arbitrarily shaped pore cross sections. *The Journal of the Acoustical Society of America*, 90(6):3228 – 3237, 1991.

[43] G. W. Swift. Streaming in thermoacoustic engines and refrigerators. *AIP Conference Proceedings*, 524(1):105–114, 2000.

[44] Arganthal Berson, Marc Michard, and Philippe Blanc-Benon. Measurement of acoustic velocity in the stack of a thermoacoustic refrigerator using particle image velocimetry. *Heat and Mass Transfer*, 44(8):1015–1023, 2008.

[45] P.C.H. Aben, P.R. Bloemen, and J.C.H. Zeegers. 2-d piv measurements of oscillatory flow around parallel plates. *Experiments in Fluids*, 46(4):631–641, 2009.

[46] Etienne Besnoin and Omar M. Knio. Numerical study of thermoacoustic heat exchangers. *Acta Acustica united with Acustica*, 90(3):432 – 444, 2004.

[47] Nathan T. Weiland and Ben T. Zinn. Open cycle traveling wave thermoacoustics: Energy fluxes and thermodynamics. *The Journal of the Acoustical Society of America*, 116(3):1507–1517, 2004.

[48] R. S. Reid, W. C. Ward, and G. W. Swift. Cyclic thermodynamics with open flow. *Phys. Rev. Lett.*, 80:4617–4620, 1998.

[49] Peter T. Landsberg. Thermodynamics: Cool sounds. *Nature*, 394:623–624, 1998.

[50] Melda Ödinç Çarpinlioglu and Mehmet Yasar Gündogdu. A critical review on pulsatile pipe flow studies directing towards future research topics. *Flow Measurement and Instrumentation*, 12(3):163 – 174, 2001.

[51] J. R. Womersley. Method for the calculation of velocity, rate of flow and viscous drag in arteries when the pressure gradient is known. *The Journal of Physiology*, 127(3):553–563, 1955.

[52] T. M. Runge, J.C. Brice no, M.E. Sheller, C.E. Moritz, L. Sloan, F.O. Bohls, and S.E. Ottmers. Hemodialysis: evidence of enhanced molecular clearance and ultrafiltration volume by using pulsatile flow. *The International Journal of Artificial Organs*, 16(9):645 – 652, 1993.

[53] Rajashekhar Pendyala, Sreenivas Jayanti, and A.R. Balakrishnan. Flow and pressure drop fluctuations in a vertical tube subject to low frequency oscillations. *Nuclear Engineering and Design*, 238(1):178 – 187, 2008.

[54] T.S. Zhao and P. Cheng. Oscillatory pressure drops through a woven-screen packed column subjected to a cyclic flow. *Cryogenics*, 36(5):333 – 341, 1996.

[55] B.P.M. Helvensteijn, A. Kashani, A.L. Spivak, P.R. Roach, J.M. Lee, and P. Kittel. Pressure drop over regenerators in oscillating flow. In Peter Kittel, editor, *Advances in Cryogenic Engineering*, volume 43 of *Advances in Cryogenic Engineering*, pages 1619–1626. Springer US, 1998.

[56] Yonglin Ju, Yan Jiang, and Yuan Zhou. Experimental study of the oscillating flow characteristics for a regenerator in a pulse tube cryocooler. *Cryogenics*, 38(6):649 – 656, 1998.

[57] Sungryel Choi, Kwanwoo Nam, and Sangkwon Jeong. Investigation on the pressure drop characteristics of cryocooler regenerators under oscillating flow and pulsating pressure conditions. *Cryogenics*, 44(3):203 – 210, 2004.

[58] Li wen Jin and KaiChoong Leong. Pressure drop and friction factor of steady and oscillating flows in open-cell porous media. *Transport in Porous Media*, 72(1):37–52, 2008.

[59] N. Riley. On a sphere oscillating in a viscous fluid. *Q. J. Mech. Appl. Math.*, 19:461 – 472, 1966.

[60] P.C. Carman. Fluid flow through granular beds. *Chemical Engineering Research and Design*, 75, Supplement:S32 – S48, 1997.

[61] K. Rietema. *The Dynamics of Fine Powders*. London: Elsevier, 1991.

[62] J. M. Valverde and A. Castellanos. Random loose packing of cohesive granular maerials. *Europhys. Lett.*, 75(6):985 – 991, 2006.

[63] Zhixiong Guo, Seo Young Kim, and Hyung Jin Sung. Pulsating flow and heat transfer in a pipe partially filled with a porous medium. *International Journal of Heat and Mass Transfer*, 40(17):4209 – 4218, 1997.

[64] Yueh-Liang Yen, Po-Chuan Huang, Chao-Fu Yang, and Yen-Jen Chen. Numerical study of heat transfer of a porous-block-mounted heat source subjected to pulsating channel flow. *Numerical Heat Transfer, Part A: Applications*, 54(4):426 – 449, 2008.

[65] Mohsen Ghafarian, Davod Mohebbi-Kalhori, and Jafar Sadegi. Analysis of heat transfer in oscillating flow through a channel filled with metal foam using computational fluid dynamics. *International Journal of Thermal Sciences*, 66:42 – 50, 2013.

[66] Shoei sheng Chen. Vibration of nuclear fuel bundles. *Nuclear Engineering and Design*, 35(3):399–422, 1975.

[67] M.P. Paidoussis. Real–life experiences with flow-induced vibration. *Journal of Fluids and Structures*, 22(6-7):741–755, 2006.

[68] Radu Pomirleanu. Harmonic analysis of a cylinder cluster in square confinement with position - dependent fluid damping. *J. Pressure Vessel Technol.*, 130:041303(1)–041303(10), 2008.

[69] W. H. Lin. ydrodynamic forces on multiple circular cylinders oscillating in a viscous incompressible fluid. *Journal of Applied Mathematics and Mechanics*, 67(10):487 501, 1987.

[70] W. Coenen and N. Riley. Oscillatory flow about a cylinder pair. *The Quarterly Journal of Mechanics and Applied Mathematics*, 62(1):53–66, 2009.

[71] G.K. Batchelor. *An Introduction To Fluid Dynamics*. Cambridge university press edition, 2002.

[72] J. Donea and A. Huerta. *Finite Element Methods for Flow Problems*. Wiley, 2003.

[73] J. Ahrens and S. Spors. Sound field reproduction using planar and linear arrays of loudspeakers. *Audio, Speech, and Language Processing, IEEE Transactions on*, 18(8):2038–2050, 2010.

[74] Blanche Dalloz-Dubrujeaud, Roland Faure, Lounés Tadrist, and Guy Giraud. Perte de pression et vitesse minimum de fluidisation dans un lit de particules 2D. *Comptes Rendus de l'Académie des Sciences - Series IIB - Mechanics-Physics-Astronomy*, 328(3):231 – 236, 2000.

[75] A.N. Brooks and T.J.R. Hughes. Streamline upwind/petrov-galerkin formulations for convection dominated flows with particular emphasis on the incompressible navier-stokes equations. *Computer Methods in Applied Mechanics and Engineering*, 32:199–259, 1982.

[76] L.P. Franca, S.L. Frey, and T.J.R. Hughes. Stabilized finite element methods: I. application to the advective-diffusive model. *Computer Methods in Applied Mechanics and Engineering*, 95(2):253–276, 1992.

[77] L.P. Franca and S.L. Frey. Stabilized finite element methods: II. the incompressible navier-stokes equations. *Computer Methods in Applied Mechanics and Engineering*, 99(2–3):209–233, 1992.

[78] E. Ramm and W. Wall. Fluid-structure interaction based upon a stabilized (ale) finite element method. Technical report, CIMNE, Barcelona, Spain, 1998.

[79] J. Chung and G. M. Hulbert. A time integration algorithm for structural dynamics with improved numerical dissipation: The generalized-a method. *J. Appl. Mech.*, 60(2):371–375, 1993.

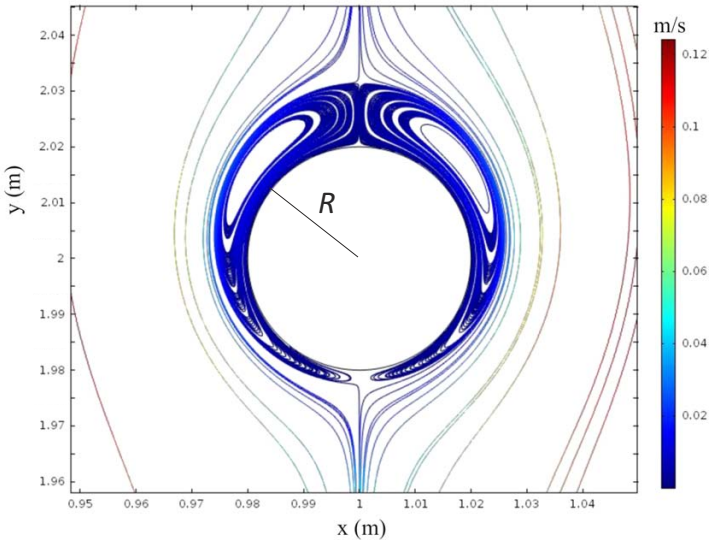

FIG. 1. Gas streamlines around a solid cylinder of infinite length (radius R=200 μm) subjected to a vertically directed sound wave of frequency 1 kHz and intensity 120 dB or, equivalently, vertically oscillating with a velocity amplitude v_1=0.07 m/s in air otherwise at rest ($\xi_1/R \simeq 0.06$, $R/\delta_v \simeq 2.9$). The cylinder is simultaneously subjected to an externally imposed gas flow (gas velocity v_g=0.1 m/s) upwards directed. Obtained by means of 3D FEM calculation as detailed in section VII

.

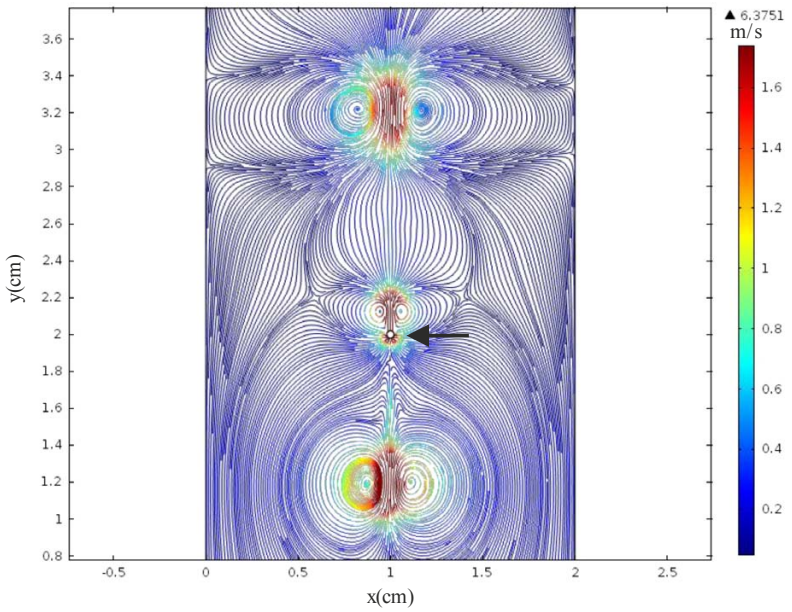

FIG. 2. Gas streamlines around a solid cylinder (instantaneous position indicated by the arrow) of infinite length (radius R=200 μm) undergoing vertical oscillations of large amplitude ($\xi_1/R \simeq 55$, $f = 100$ Hz, $v_1 \simeq 7$ m/s, $R/\delta_v \simeq 1$) or, equivalently, subjected to a sound wave of high intensity ($SIL \simeq 160$ dB). The cylinder is simultaneously subjected to an externally imposed gas flow (gas velocity v_g=0.1 m/s) upwards directed. Boundary layer detachment and wake flows are illustrated. Obtained by means of 3D FEM calculation as detailed in section VII

.

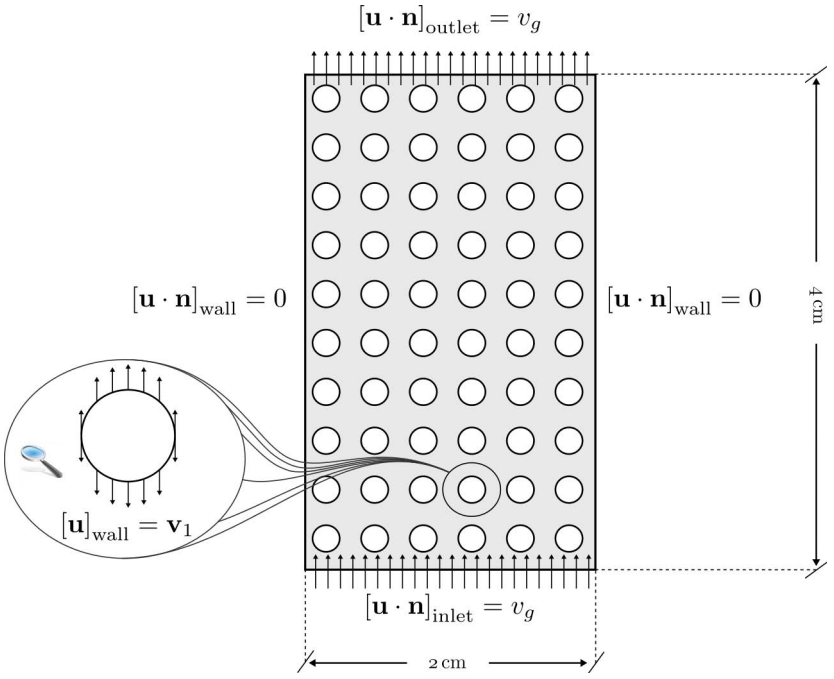

FIG. 3. Schematic representation of the system used for the numerical study. The array of 17×33 solidary cylinders (of radius $R = 200$ μm) is placed between solid walls separated by a distance of 2 cm. The cylinders are vertically oscillated (oscillation velocity amplitude v_1) and subjected to an externally imposed gas flow (superficial velocity v_g.

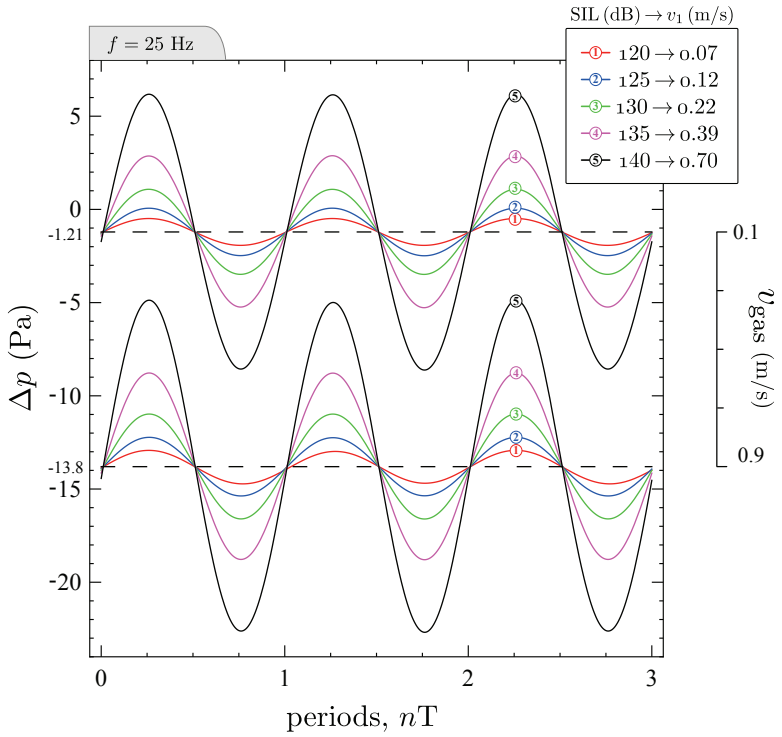

FIG. 4. Gas pressure drop across the oscillating array of cylinders (oscillation frequency $f = 25Hz$) numerically derived as a function of time (made nondimensional with the oscillation period $T = 1/f$) for different values of the oscillation velocity (v_1) or, equivalently, SIL values (as indicated) and for different superficial velocities (v_g=0.1 m/s and 0.9 m/s) of the externally imposed gas flow.

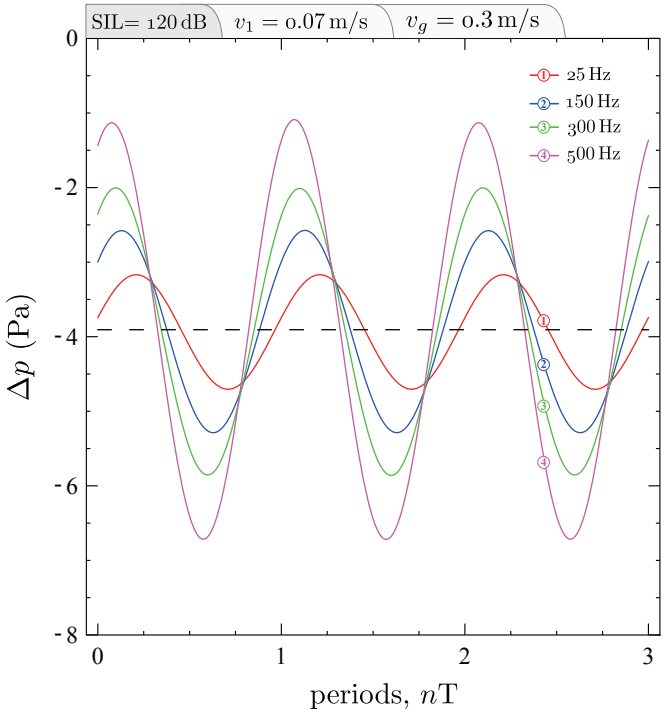

FIG. 5. Gas pressure drop across the oscillating array of cylinders numerically derived as a function of time (made nondimensional with the oscillation period $T = 1/f$) for different values of the oscillation frequency as indicated. The oscillation velocity is fixed to $v_1 = 0.07$ m/s (SIL=120 dB) as well as the velocity of the externally imposed gas flow (v_g=0.3 m/s).

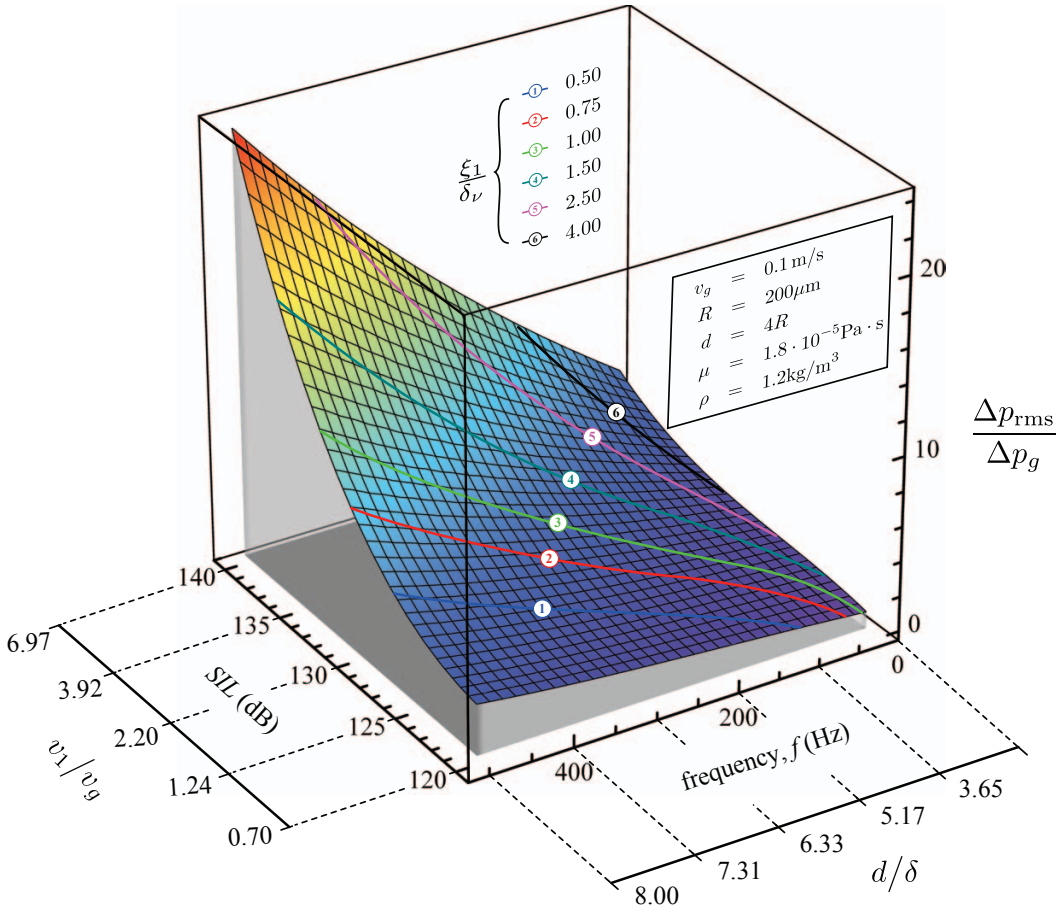

FIG. 6. Ratio of cycle-averaged gas pressure drop to steady component of the pressure drop across the oscillating array of cylinders as a function of the oscillation frequency and SIL value when the velocity of the externally imposed gas flow is $v_g = 0.1$ m/s. Additional horizontal axes show the equivalent values of the ratio of the interparticle separation distance to the viscous boundary layer thickness (d/δ_ν) and the ratio of the oscillation velocity amplitude to the external gas flow velocity (v_1/v_g). Contour lines indicate constant values of the ratio of the oscillation amplitude ξ_1 to δ.

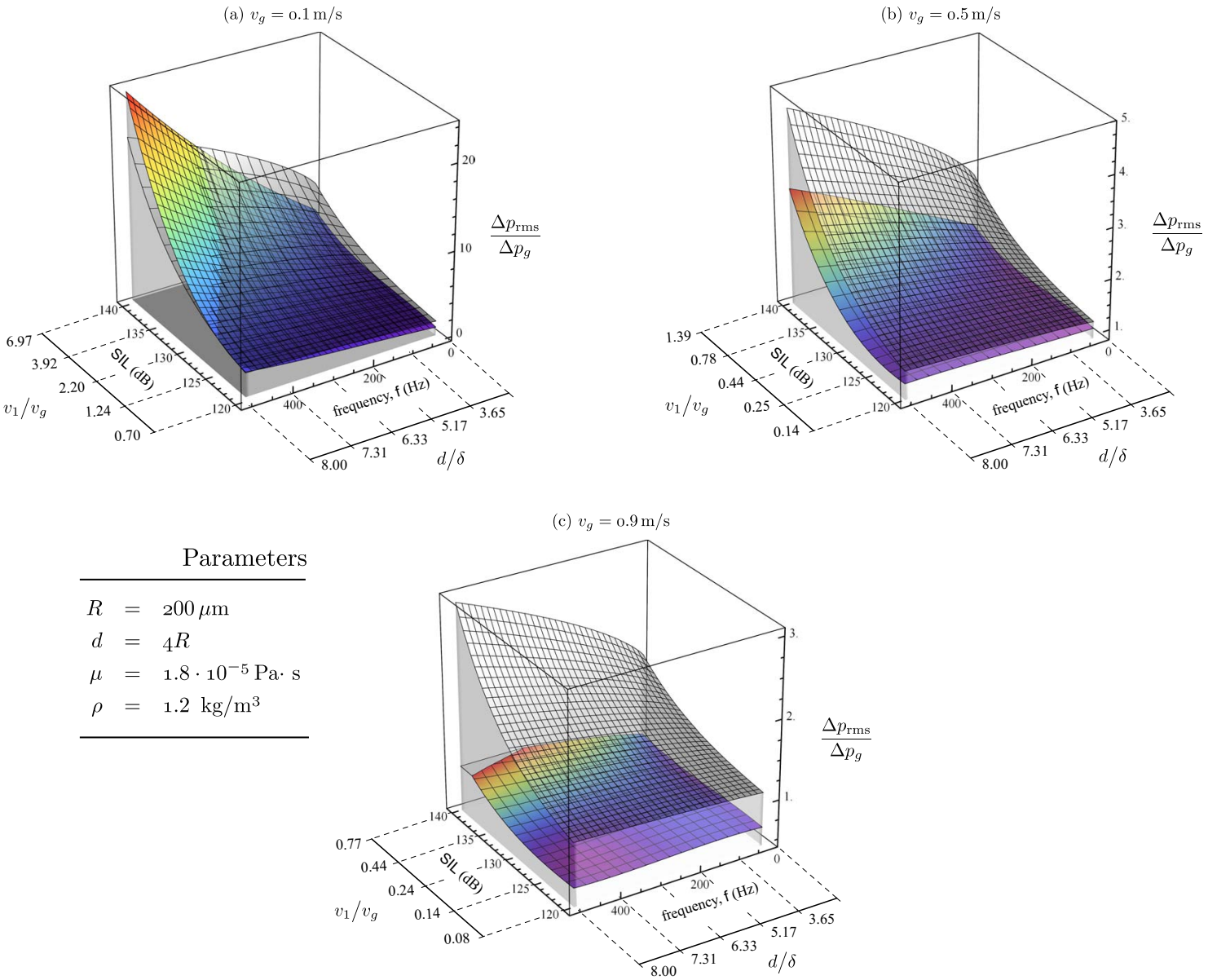

Parameters

R	=	$200\,\mu\mathrm{m}$
d	=	$4R$
μ	=	$1.8 \cdot 10^{-5}\,\mathrm{Pa}\cdot\,\mathrm{s}$
ρ	=	$1.2\ \mathrm{kg/m^3}$

FIG. 7. Ratio of cycle-averaged to steady gas pressure drop across the oscillating array of cylinders as a function of the oscillation frequency and SIL values for different values of the external gas flow velocity (a:$v_g = 0.1$ m/s, b: v_g=0.5 m/s, b: $v_g = 0.9$ m/s). Numerical results are plotted using color graded surface. Theoretically predicted results (Eq. 15) are shown by the grey graded surface.

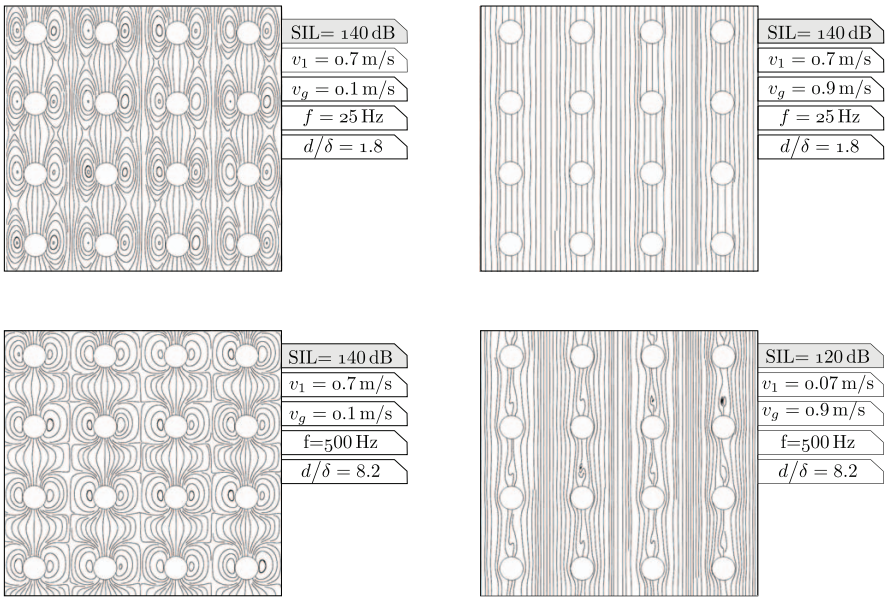

FIG. 8. Snapshots of gas streamlines within the array of oscillating cylinders for different values of the superficial velocity of the externally imposed gas flow v_g and oscillation velocity amplitude v_1 (or, equivalently sound intensity level SIL) as indicated.

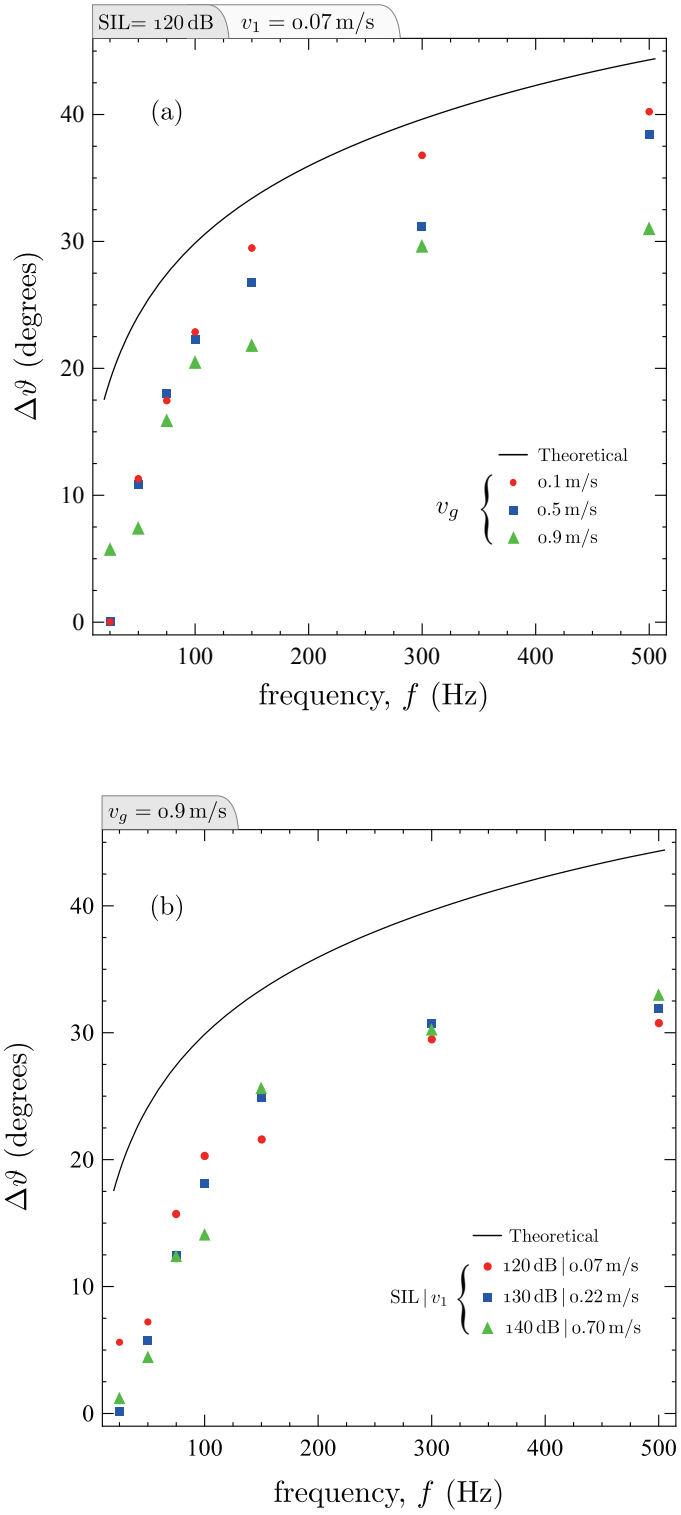

FIG. 9. Phase shift between the gas pressure drop across the oscillating array of cylinders and velocity oscillation as a function of the oscillation frequency. In (a) phase shift data are plotted for different values of the external gas velocity v_g and fixed oscillation amplitude v_1. (b) shows the phase shift for different values of the oscillation velocity amplitude v_1 and a fixed gas velocity v_g. The solid line is the theoretical prediction by Eq. 12.

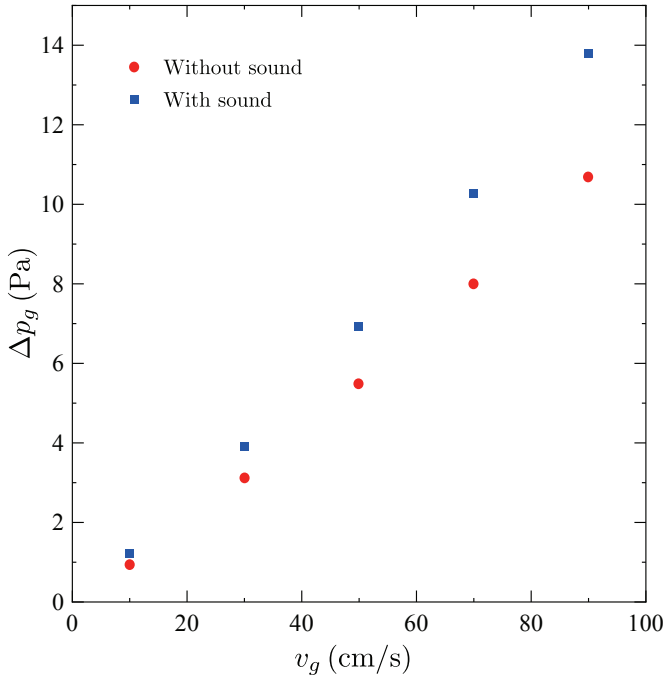

FIG. 10. a) Steady component of the pressure drop across the array of cylinders as a function of the superficial velocity of the externally imposed gas flow v_g, subjected to a sound wave (SIL=140 dB) and in the absence of sound wave.

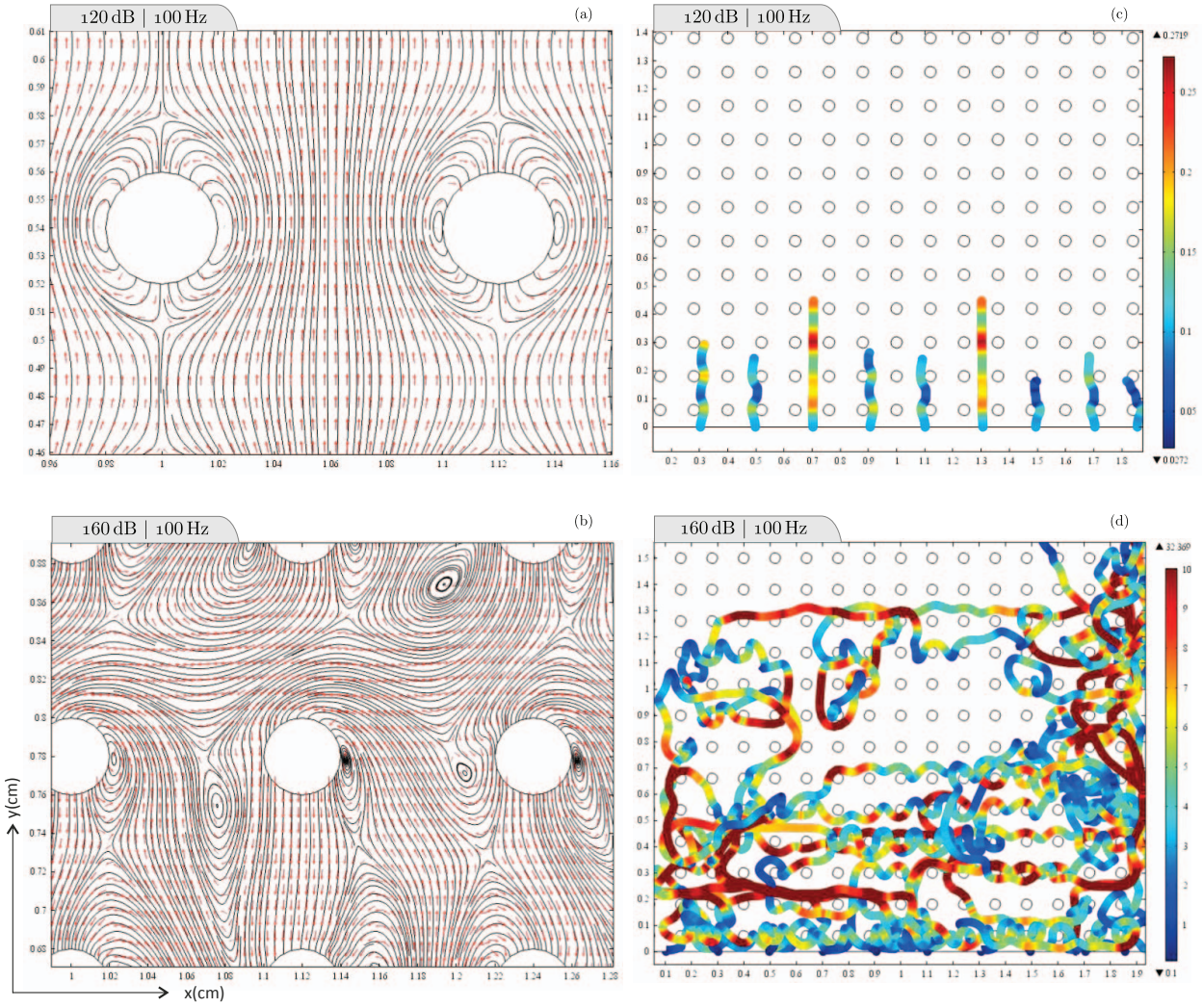

FIG. 11. a), b): Snapshots of gas flow streamlines within the array of oscillating cylinders (f =100 Hz) for SIL=120 dB ($v_1 \simeq 0.07$ m/s) and 160 dB ($v_1 \simeq 7$ m/s) as indicated. External gas flow velocity $v_g = 0.1$ m/s. c) and d): Trajectories of tracers introduced in the external gas flow.

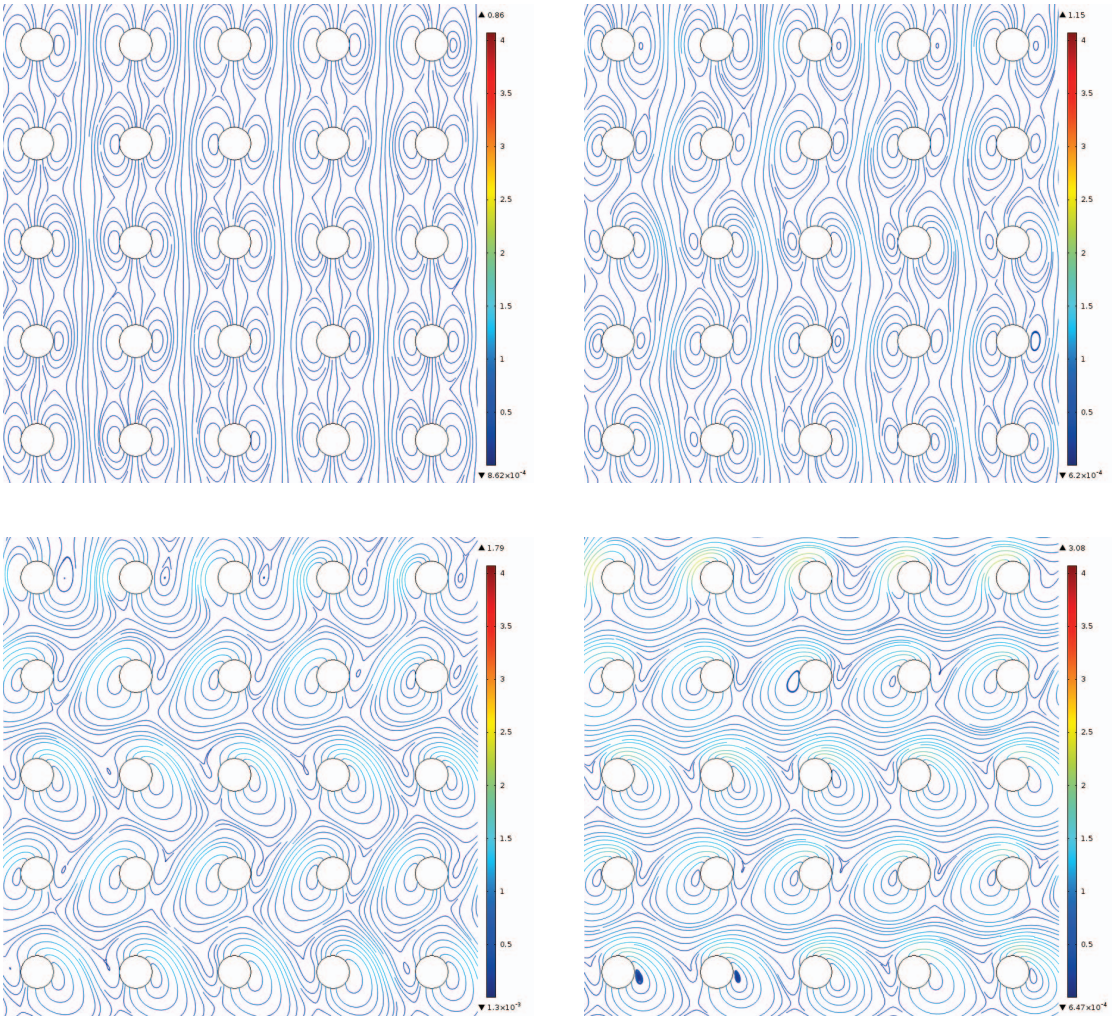

FIG. 12. Snapshots of gas flow streamlines within the array of oscillating cylinders (SIL=140 dB, $v_1 \simeq 0.7$ m/s, $f = 25$ Hz, $v_g = 0.1$ m/s) illustrating the interference between boundary layers as caused by an increase of the air temperature up to 900°C ($d/\delta_\nu = 0.56$).

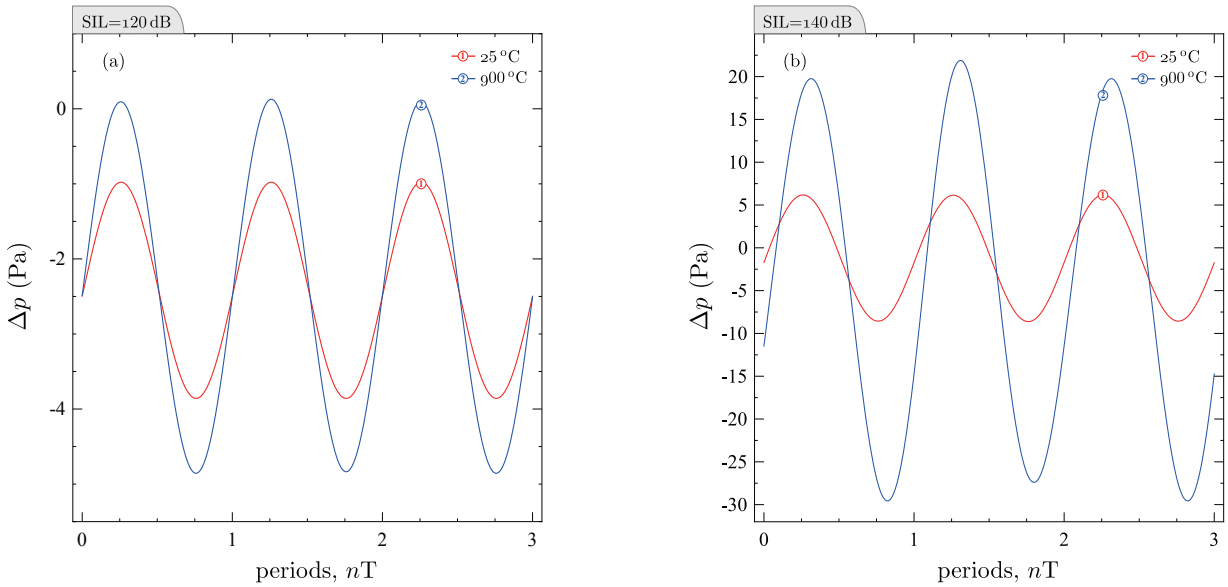

FIG. 13. Gas pressure drop across the oscillating array of cylinders numerically derived as a function of time (made nondimensional with the oscillation period $T = 1/f$) for different values of air temperature. The oscillation velocity is fixed to $v_1 = 0.07$ m/s (SIL=120 dB) in a) and $v_1 = 0.7$ m/s (SIL=140 dB) in b). The velocity of the externally imposed gas flow is fixed to v_g=0.1 m/s).